

# Microcalcification Detection in Mammography using Wavelet Transform and Statistical Parameters

Eliza Hashemi Aghjekandi

## Abstract

The earliest sign of breast cancer is the existence of microcalcifications which are tiny calcium clusters in breast tissues detected in mammographies. Early detection and diagnosis of microcalcifications is the main step to improve prognosis of breast cancer, which is one of the most frequently serious disease among women. In this work, we study the methodology based on Bi-dimensional discrete wavelet transform and statistical measurements to estimate the position of these tiny clusters in mammographies. The statistical analysis involves calculating skewness and kurtosis values of all three sets of wavelet coefficients. The crossing of rows and columns associated to the high skewness and kurtosis values determine regions of microcalcifications clusters. Simulation results show that the investigated methodology is successful in the majority of the 18 analyzed images containing tumors.

**Key Words:** Microcalcifications in Mammography, Wavelets Transforms, Skewness and Kurtosis Parameter.

## Acknowledgment

My deepest gratitude goes first to my examiner and supervisor Mohammad Asadzadeh and Alice Kozakevicius, for their support and guidance. I would like to thank them for their invaluable comments and instructions. I also would like to thank the professors and teachers at department of Mathematics.

Finally I wish to mention my appreciation to my beloved family for their loving encouragement through these years.

# Contents

<b>1</b>	<b>Introduction</b>	<b>3</b>
<b>2</b>	<b>Wavelet Framework</b>	<b>5</b>
2.1	Multiresolution Analysis . . . . .	5
2.1.1	Properties of Scaling and Wavelet Functions . . . . .	7
2.1.2	Scaling and Wavelet Equations . . . . .	7
2.1.3	Vanishing Moments . . . . .	8
<b>3</b>	<b>One Dimensional Discrete Wavelet Transform</b>	<b>9</b>
3.1	Wavelet Expansions . . . . .	9
3.2	Discrete Wavelet Transform . . . . .	10
3.2.1	Daubechies Wavelet Transform . . . . .	11
3.2.2	Haar Wavelet Transform . . . . .	15
3.2.3	Cascade Algorithm . . . . .	16
3.2.4	Boundary problem . . . . .	17
<b>4</b>	<b>Two Dimensional Discrete Wavelet System</b>	<b>29</b>
4.1	Two Dimensional Scaling and Wavelet Functions . . . . .	29
4.2	Two Dimensional Wavelet Transform . . . . .	30
<b>5</b>	<b>Microcalcifications detection in Mammography</b>	<b>36</b>
5.1	Wavelets Representation of Images . . . . .	36
5.2	Thresholding . . . . .	37
5.2.1	Soft Thresholding . . . . .	37
5.2.2	Hard thresholding . . . . .	38
5.3	Detection Parameters: Skewness and Kurtosis . . . . .	39
5.3.1	Numerical Experiments . . . . .	40
5.4	Result and Discussion . . . . .	52
<b>6</b>	<b>Conclusion</b>	<b>53</b>
	<b>References</b>	<b>55</b>

# 1 Introduction

Breast cancer is the most frequently diagnosed type, which ranks first place as a cause of cancer death in women. Since 1990 the rates for breast cancer death, according to statistics collected in USA [5], have been decreasing about 3 percent per year exactly due to earlier detection of the disease. The early diagnosis of malignant tumors can contribute for the survival of patients up to 98 percent, which can be detected by mammogram before any abnormal feeling by patients.

A mammography is a specific type of imaging that uses a low-dose x-ray system to examine breasts and a mammography exam is called a mammogram [18]. One of the indicators of breast cancer searched in mammograms are clusters formed by microcalcifications, tiny calcium deposits in breast tissues, that appear as small bright spots in the imaging [18].

In the last 15 years several mammography processing methods have been developed in order to detect microcalcifications by radiologists, among them wavelet based methods have been used efficiently. A wavelet transform is a powerful tool to analyze and to identify strong variations contained within the original data, since in each level of the transform data is divided into different scaling components. This main property is therefore explored in many applications, where different behaviors have to be highlighted and recognized during the analysis [2, 3].

There is a large number of wavelet families, for example the functions introduced by Meyer [10], which are suitable for continuous transformations. Another example is the orthonormal set of functions with compact support defined by Ingrid Daubechies [3]. They create a framework for representing elements in the space of the square integrable functions  $L^2(\mathbb{R})$ , which in fact contains the finite signals analyzed in this work. The representation of any element in  $L^2(\mathbb{R})$  is obtained by wavelet expansions in time and resolution levels of these elements. According to [3], the Daubechies wavelet family is connected to filter bank methods in digital signal processing, and therefore they are used for discrete and fast transformations. The 1:1 relation between Daubechies wavelets and finite sized filters makes this family very important in the analysis of discrete signals.

There are many types of fast algorithms for computing the discrete wavelet transform [8]. Basically they can be divided into two groups: decimated and undecimated algorithms. In the decimated case, each time a new decomposition level is calculated, the input vector with discrete data is splitted in two other vectors with half of the size from the original one. In the undecimated case, all vectors remain with the same size during the entire factorization process. In this work the decimated version for the fast wavelet transform, called Mallat Cascade algorithm, is considered for one and two dimensions [8]. Nevertheless, in the analysis of mammograms not only the Cascade algorithm is explored, versions of the undecimated case are used with different families of filter banks.

Examples of analysis considering undecimated algorithms are presented in [11, 14]. In [11] the mammogram image is first processed by a subband decomposition filter bank, and the resulting subimages are divided into overlapping square regions. In [14] the same kind of overlapping blocks are obtained, but this time the simplest Daubechies wavelets, called Haar functions, are used in the transformation. According to [15],

microcalcifications in mammograms correspond to high frequency coefficients of the image spectrum, and in this case they are related to wavelet coefficients in the highest levels of the factorization. One simple method to detect and to extract calcifications is to decompose the mammography by wavelet transforms, suppressing the low frequency subband (scaling coefficients block from the lowest level), and reconstruct data considering only the high frequency associated wavelet coefficients. In [15] the decimated algorithm for the Daubechies wavelet transform with 2 and 10 null moments is used. Unfortunately this procedure can lead to a high number of false positive results (wrongly cancer detected regions).

An attempt to reduce the number of false positives is to include statistical parameters during some stage of the wavelet analysis. According to [14], in microcalcifications regions the symmetry of the Gaussian distribution of wavelet coefficients is destroyed and the tails of their distribution are heavier. The statistical quantities able to identify these deformations in the shape of the Gaussian distributions are the third and fourth order correlation parameters, called skewness and kurtosis, respectively. In [11, 14] the analysis explores both kurtosis and skewness computations for overlapping blocks. The detection problem is then posed as a hypothesis test in which areas with the skewness and the kurtosis values greater than threshold values are considered as regions of microcalcifications. Experimental studies showed that this method was successful in detecting regions containing microcalcifications.

In the present work, the methodology for detecting microcalcifications in mammography differs from the one presented in [11, 14], since here the discrete Daubechies wavelet transform with 2 null moments and statistical measurements are applied. Another difference is that now the decimated algorithm for Daubechies wavelet transform is considered, avoiding the arise of overlapping subregions. For each row and column of the sets of wavelet coefficients (also called wavelet subbands), skewness and kurtosis values are computed. The vectors containing these values are then thresholded. The significant values, those greater than threshold parameters are kept. The crossing of common lines and columns (for both skewness and kurtosis calculations) associated to the significant values determine candidate regions of microcalcifications clusters.

This work is organized as follows: In section II we present a review of wavelet framework and multiresolution analysis, the scaling and wavelet functions for orthonormal Daubechies family of compact support and some of their essential properties are presented. Section III and IV present one and two dimensional discrete wavelet transform for Daubechies wavelet families. The simplest example for this family of transformations, the Haar wavelet transform, is also exemplified. At the end of section III, three possibilities for the data extension on the boundaries are presented to circumvent the problems at the boundaries occurred by Daubechies wavelet transform with more than 2 null moments, when finite signals are analyzed. In section V some methodologists based on the decimated Db2 wavelet transform and statistical algorithms proposed in [11, 14] are studied. In this section 24 images obtained from the University of South Florida Digital Mammography Home page [18] are analyzed with the modified algorithm presented in the subsection 5.3. The numerical results show that the aforesaid method with the negligible rate of false positive numbers is successful in detecting regions containing microcalcifications. Finally a table resulting from tests on a set of 24 digital mammographies where 18 of them identify microcalcifications is presented.

## 2 Wavelet Framework

The wavelet transform is a mathematical tool with a great variety of applications, and one important example, given by Mallat [8], is signal and image analysis. By a wavelet transform data can be splitted into different scaling components and then each component is analyzed with a resolution matched to its scale [3]. There are many types of wavelet families, for example functions suitable for continuous transformations [10] and the orthonormal set of functions with compact support, which define an important group of discrete wavelet transforms [3], spline -wavelets and many others [3, 8].

In this work the family of orthonormal wavelets with compact support defined by Ingrid Daubechies [3] is considered. This family of functions defines an orthonormal basis for the space of square integrable functions

$$L^2(\mathbb{R}) = \{f : \mathbb{R} \rightarrow \mathbb{C} : \int_{\mathbb{R}} |f(x)|^2 < \infty\}.$$

The construction of the Daubechies wavelets is based on a specific framework called multiresolution analysis [8, 10], which is a set of properties necessary not only for the construction of the basis on  $L^2(\mathbb{R})$ , but also for the definition of the family itself, the relation between scales, and the obtainment of the wavelet transform.

In this section the Multiresolution analysis is defined according to definitions presented by Ingrid Daubechies in [3]. Nevertheless no filter construction is presented. The filters are directly considered defined from the list provided in [3]. The main goal is to point out how the discrete wavelet transform can be derived from the scaling relations defined by this framework.

### 2.1 Multiresolution Analysis

#### Definition 2.1.

According to [3], a *multiresolution analysis* (MRA) is a family of subspaces  $V_j \in L^2(\mathbb{R})$  that satisfies the following properties:

**I. Monotonicity**

The sequence is increasing,  $V_j \subset V_{j+1}$  for all  $j \in \mathbb{Z}$ .

**II. Existence of the Scaling Function**

There exists a function  $\varphi \in V_0$ , such that the set  $\{\varphi(\cdot - k) : k \in \mathbb{Z}\}$  is an orthonormal basis for  $V_0$ .

**III. Dilation Property**

For each  $j$ ,  $f(x) \in V_0$  if and only if  $f(2^j x) \in V_j$ .

**IV. Trivial Intersection Property**

$\bigcap_{j \in \mathbb{Z}} V_j = \{0\}$ .

**V. Density**

$\overline{\bigcup_{j \in \mathbb{Z}} V_j} = L^2(\mathbb{R})$ .

Condition I shows that a multiresolution analysis consists of a sequence of approximation spaces  $V_j$  where

$$0 \subset \cdots \subset V_{-1} \subset V_0 \subset V_1 \subset \cdots \subset L^2(\mathbb{R}).$$

Condition II states that the approximation spaces are spanned by functions  $\varphi$ , which is called the *scaling function* of the multiresolution analysis, so different choices for  $\varphi$  yield different multiresolution analysis. And

$$\|\varphi\|_{L^2} = \left( \int_{-\infty}^{+\infty} |\varphi(x)|^2 dx \right)^{\frac{1}{2}} = 1.$$

For all  $j, k \in \mathbb{Z}$ , the dilation, translation and normalization is given by

$$\varphi_{j,k}(x) = 2^{j/2} \varphi(2^j x - k).$$

Conditions II and III together imply that  $\{\varphi_{j,k} : k \in \mathbb{Z}\}$  is an orthonormal basis for  $V_j$  for all  $j \in \mathbb{Z}$ .

For every  $j \in \mathbb{Z}$ ,  $W_j$  is defined to be the orthogonal complement of  $V_j$  in  $V_{j+1}$ . It means that

$$V_j \perp W_j \quad , \quad V_j \oplus W_j = V_{j+1}. \quad (2.1)$$

Applying (2.1) recursively for  $J > J_0$  follows that

$$V_J = V_{J_0} \oplus W_{J_0} \oplus \cdots \oplus W_{J-1}, \quad (2.2)$$

where all the involved subspaces are orthogonal. Continuing the decomposition (2.2), and letting  $J_0 \rightarrow -\infty$  and  $J \rightarrow +\infty$  yields

$$L^2(\mathbb{R}) = \bigoplus_{j \in \mathbb{Z}} W_j.$$

It means that  $W_j$ 's are orthogonal. As Shown in [3], there exists a function  $\psi(x) \in W_0$  such that  $\{\psi(2x - k)\}_{k \in \mathbb{Z}}$  is an orthonormal basis for  $W_0$ . So according to the multiresolution analysis properties, the whole collection  $\{\psi_{j,k}; j, k \in \mathbb{Z}\}$ ,

$$\psi_{j,k}(x) = 2^{j/2} \psi(2^j x - k),$$

is an orthonormal basis for  $L^2(\mathbb{R})$ .  $\psi(x)$  is called *wavelet function*.

An example of spaces  $V_j$  satisfying the aforesaid conditions in [3] is

$$V_j = \{f \in L^2(\mathbb{R}) : f \text{ is constant on } [2^{-j}k, 2^{-j}(k+1)), \quad \forall j, k \in \mathbb{Z}\},$$

where it is called the *Haar multiresolution analysis*, and a possible choice for  $\varphi$  is the indicator function for  $[0, 1)$ . In this case  $\varphi$  is called the *Haar scaling function* of the multiresolution analysis, and the function  $\varphi(x - k)$  has the same graph as  $\varphi$ , Figure 3a, but translated  $k$  units to the right. Since  $\varphi(x - k)$  is discontinuous at  $x = k$  and  $x = k + 1$ , and  $k$  ranges over a finite set, so each element of  $V_0$  is zero outside a bounded set. It means that  $\varphi$  has *finite or compact support* ( the other Daubechies constructions of the

wavelet system are compactly supported and continuous). Also for  $k \neq k'$ ,  $\varphi(x-k')$  and  $\varphi(x-k)$  have disjoint supports, therefore the set  $\{\varphi(x-k)\}_{k \in \mathbb{Z}}$  is an orthonormal basis for  $V_0$ .

In general, The Haar scaling function generates the subspaces  $V_j$ , which are discontinuous in the set of integer multiples of  $2^{-j}$ . The scaling condition for the Haar system (special case of the Daubechies system) satisfies the condition III, so the Haar system of  $V_j$  satisfies all the properties of a multiresolution analysis.

### 2.1.1 Properties of Scaling and Wavelet Functions

According to the condition of multiresolution analysis,  $\{\varphi(x-k)\}_{k \in \mathbb{Z}}$  is an orthonormal basis for  $V_0$ .

The first and third conditions imply that  $\{\varphi(2x-k)\}_{k \in \mathbb{Z}}$  is a basis of  $V_1$ , and by substituting  $2x = y$  we have

$$\int_{-\infty}^{+\infty} \varphi(2x-k)dx = \frac{1}{2} \int_{-\infty}^{+\infty} \varphi(y-k)dy = \frac{1}{2} \int_{-\infty}^{+\infty} \varphi(\tilde{x})d\tilde{x}. \quad (2.3)$$

The scaling function has the mass equal to one,[1], i.e.

$$\int_{-\infty}^{+\infty} \varphi(x)dx = 1,$$

so the equation (2.3) yields

$$\int_{-\infty}^{+\infty} \varphi(2x-k)dx = \frac{1}{2}.$$

Therefore  $\|\varphi(2x-k)\|_{L_2} = \frac{1}{\sqrt{2}}$ , and the normalized case is

$$\frac{\varphi(2x-k)}{\|\varphi(2x-k)\|_{L_2}} = \sqrt{2}\varphi(2x-k).$$

Hence  $\{2^{1/2}\varphi(2x-k)\}_{k \in \mathbb{Z}}$  is an orthonormal basis of  $V_1$ . Recursively,  $\{2^{j/2}\varphi(2^jx-k)\}_{k \in \mathbb{Z}}$  is orthonormal basis for  $V_j$ .

Also for the wavelet space  $W_j$ ,  $\{2^{j/2}\psi(2^jx-k)\}_{k \in \mathbb{Z}}$  is an orthonormal wavelet basis.

### 2.1.2 Scaling and Wavelet Equations

Since  $V_0 \subset V_1$ , any function  $f$  in  $V_0$  can be expanded in term of the basis function for  $V_1$ . So in particular the scaling function  $\varphi(x) \in V_0$  and the wavelet function  $\psi \in V_1$  can be written as:

$$\varphi(x) = \sum_{k \in \mathbb{Z}} h_k \varphi_{1,k}(x) = 2^{1/2} \sum_{k \in \mathbb{Z}} h_k \varphi(2x-k), \quad (2.4)$$

and

$$\psi(x) = 2^{1/2} \sum_{k \in \mathbb{Z}} g_k \varphi(2x-k), \quad (2.5)$$

where

$$h_k = \int_{-\infty}^{+\infty} \varphi(x) \varphi_{1,k}(x) dx, \quad g_k = \int_{-\infty}^{+\infty} \psi(x) \varphi_{1,k}(x) dx,$$

and

$$\sum_{k \in \mathbb{Z}} |h_k|^2 = \sum_{k \in \mathbb{Z}} |g_k|^2 = 1.$$

Equation (2.4), (2.5) are called the *scaling* and *wavelet equation*, respectively. For a scaling function with compact support defined by Haar and Daubechies ([1], [2]), only a finite number of (filter) coefficients  $h_k$  and  $g_k$  are non zero.

Therefore, for the case of wavelets with compact support, scaling equation defined as:

$$\varphi(x) = 2^{1/2} \sum_{k=0}^{D-1} h_k \varphi(2x-k),$$

where  $D \in \mathbb{N}$  is called the *wavelet genus*, and the numbers  $h_0, h_1, \dots, h_{D-1}$  are called *filter coefficients*.

According to [3], since  $\psi \in W_0 \subset V_1$ , the same property holds for  $\psi$

$$\psi(x) = 2^{1/2} \sum_{k=0}^{D-1} g_k \varphi(2x-k),$$

where  $g_k = (-1)^k h_{D-1-k}$ , for  $k = 0, 1, \dots, D-1$ , and  $\sum_{k=0}^{D-1} h_k g_k = 0$ .

Ingrid Daubechies in [3] computed this relations and obtained discrete values for the filters  $h_k, g_k$  according to the properties imposed to the multiresolution analysis. Therefore the filters are uniquely related to the choice of  $\varphi, \psi$  for the wavelet basis.

### 2.1.3 Vanishing Moments

Here we explain the important property of wavelets which produces their capability in compressing data [1].

According to [1], the scaling function  $\varphi$  has the approximation property when it reproduces exactly polynomials up to order  $N-1$ ,

$$\sum_k M_k^p \varphi(x-k) = x^p, \quad \text{for } p = 0, \dots, N-1.$$

The integer  $N$  is the order of the multiresolution analysis.  $M_k^p$  is the  $p$ th moment of  $\varphi(x-k)$ .

Consider  $x^p \in V_j$ , since  $V_j \perp W_j$ , so  $\langle x^p, \psi_{j,k} \rangle = 0$ , for every wavelet function  $\psi_{j,k}$  and

$$\int_{-\infty}^{+\infty} x^p \psi(x) dx = \sum_k M_k^p \int_{-\infty}^{+\infty} \varphi(x-k) \psi(x) dx = 0,$$

for  $p = 0, \dots, N-1$ . It means that the wavelet  $\psi$ , associated to the scaling function  $\phi$ , has  $N$  *vanishing moments*.

According to the properties stated by the Multiresolution framework, Scaling and wavelet functions with compact support are specially suitable for the decomposition and the reconstruction of data in many resolution levels.

### 3 One Dimensional Discrete Wavelet Transform

In this section we focus on the main property of wavelets: decomposition and reconstruction of a function in  $L^2(\mathbb{R})$  (e.g. a signal or an image) in terms of its wavelet series, and we point out the relation between coefficients in approximation and wavelet spaces and the filters associated to the functions  $\varphi$  and  $\psi$ . With this the discrete wavelet transform is presented.

#### 3.1 Wavelet Expansions

According to the MRA presented in Section 2,  $L^2(\mathbb{R}) = \bigoplus_{j=-\infty}^{+\infty} W_j$ . So if we denote  $V_{J_0} = \bigoplus_{j=-\infty}^{J_0-1} W_j$ , then

$$L^2(\mathbb{R}) = V_{J_0} \oplus \bigoplus_{j=J_0}^{+\infty} W_j.$$

Therefore, any function  $f \in L^2(\mathbb{R})$  can be written in the wavelet basis as

$$f(x) = \sum_{k=-\infty}^{+\infty} c_{J_0,k} \varphi_{J_0,k}(x) + \sum_{j=J_0}^{+\infty} \sum_{k \in \mathbb{Z}} d_{j,k} \psi_{j,k}(x), \quad (3.1)$$

where  $J_0$  is considered the lowest level of representation of the function, and

$$c_{J_0,k} = \langle f, \varphi_{J_0,k} \rangle, \quad d_{j,k} = \langle f, \psi_{j,k} \rangle, \quad (3.2)$$

are scaling and wavelet coefficients of the wavelet expansions, respectively.

According to [1], the approximation  $f_{J_0} \in V_{J_0}$  of a function  $f \in L^2(\mathbb{R})$  is the orthogonal projection onto  $V_{J_0}$  (which is denoted by  $P_{J_0}$ ). Therefore

$$f_{J_0}(x) = P_{J_0}f(x) = \sum_{k=-\infty}^{+\infty} c_{J_0,k} \varphi_{J_0,k}(x). \quad (3.3)$$

The error in this approximation is given by

$$e_J = f(x) - P_J f(x) = \sum_{j=J_0+1}^{+\infty} \sum_{k=-\infty}^{+\infty} d_{j,k} \psi_{j,k}(x).$$

Since  $V_J = V_{J-1} \oplus W_{J-1}$ , the projection  $P_J f$  can be

$$P_J f(x) = \sum_{l=-\infty}^{+\infty} c_{J-1,l} \varphi_{J-1,l}(x) + \sum_{l=-\infty}^{+\infty} d_{J-1,l} \psi_{J-1,l}(x).$$

Where according to the scaling equation (2.4)

$$\varphi_{J-1,l}(x) = 2^{\frac{J-1}{2}} \varphi(2^{J-1}x - l) = 2^{\frac{J}{2}} \sum_{k=0}^{D-1} h_k \varphi(2^J x - 2l - k) = \sum_{k=0}^{D-1} h_k \varphi_{J,2l+k}(x). \quad (3.4)$$

And similarly by the wavelet equation we have

$$\psi_{J-1,l}(x) = \sum_{k=0}^{D-1} g_k \varphi_{J,2l+k}(x).$$

Therefore, by equations (3.2) and (3.4) we have

$$c_{J-1,l} = \int_{-\infty}^{+\infty} f(x) \varphi_{J-1,l}(x) dx = \int_{-\infty}^{+\infty} f(x) \left( \sum_{k=0}^{D-1} h_k \varphi_{J,2l+k}(x) \right) dx = \sum_{k=0}^{D-1} h_k c_{J,2l+k},$$

and similarly

$$d_{J-1,l} = \sum_{k=0}^{D-1} g_k c_{J,2l+k}.$$

### 3.2 Discrete Wavelet Transform

Now consider  $f : I \rightarrow L^2(I)$ , the expansion 3.1 no longer has variation for  $k$  from  $-\infty$  to  $+\infty$ .

Assume that we have a function  $f_j \in V_j$ . Since  $V_j = V_{j-1} \oplus W_{j-1}$ ,  $f_j$  can be splitted into its orthonormal components in  $V_{j-1}, W_{j-1}$

$$f(x) = \sum_{l=0}^{N_{j-1}-1} c_{j-1,l} \varphi_{j-1,l}(x) + \sum_{l=0}^{N_{j-1}-1} d_{j-1,l} \psi_{j-1,l}(x),$$

where according to the scaling equation (2.4) we obtain

$$c_{j-1,l} = \sum_{k=0}^{D-1} h_{k-2l} c_{j,k}, \quad \text{and} \quad d_{j-1,l} = \sum_{k=0}^{D-1} h_{k-2l} d_{j,k},$$

with  $c_{j,l} = f_j(x_l)$  for  $l = 0, \dots, N_j - 1$  and  $N_j = 2^{N_{max}}$ .

Repeat this process recursively, starting with the coefficients  $c_{j,l}$ , this gives the wavelet and scaling coefficients  $d_{j-1,l}$  and  $c_{j-1,l}$  for  $j = j, j-1, \dots, j-L$  and  $l = 0, \dots, \frac{N_j}{2} - 1$ .

According to [1] this recursive scheme is called the *fast forward wavelet transform*, and it is used to *decompose* a function in  $L$  levels.

Since we compute  $c_{j-1,l}, d_{j-1,l}$  from  $c_{j,k}$ , the coefficients  $c_{j,k}$  can be reconstructed by coefficients  $c_{j-1,l}$  and  $d_{j-1,l}$  associated to  $V_{j-1}$  and  $W_{j-1}$  spaces,

$$c_{j,k} = \langle f_j, \varphi_j \rangle = \sum_{l=\lceil \frac{k-D+1}{2} \rceil}^{\lfloor \frac{k}{2} \rfloor} h_{k-2l} c_{j-1,l} + \sum_{l=\lceil \frac{k-D+1}{2} \rceil}^{\lfloor \frac{k}{2} \rfloor} g_{k-2l} d_{j-1,l}.$$

So from  $c_{j-L,l}$  and  $d_{j-L,l}$ , we can reconstruct  $c_{j-L+1,l}$ , and so on, until the highest level is achieved. This is called *fast inverse wavelet transform*.

### 3.2.1 Daubechies Wavelet Transform

In this section we focus on the specific example of Daubechies wavelets transform based on the scaling and wavelet function with 2 vanishing moments, which define filters with  $D = 4$  coefficients denoted as **Db2**. The scaling filters are given by

$$h_0 = \frac{1 + \sqrt{3}}{4}, \quad h_1 = \frac{3 + \sqrt{3}}{4}, \quad h_2 = \frac{3 - \sqrt{3}}{4}, \quad h_3 = \frac{1 - \sqrt{3}}{4}.$$

Since wavelet function is orthogonal to scaling function, the scaling and wavelet filter coefficients are related as:

$$g_0 = h_3, \quad g_1 = -h_2, \quad g_2 = h_1, \quad g_3 = -h_0.$$

In this case ,one may easily check that:

$$h_0^2 + h_1^2 + h_2^2 + h_3^2 = 1, \quad (3.5)$$

$$h_0 h_2 + h_1 h_3 = 0. \quad (3.6)$$

$$h_0 + h_1 + h_2 + h_3 = 2, \quad (3.7)$$

$$g_0^2 + g_1^2 + g_2^2 + g_3^2 = 1,$$

$$g_0 + g_1 + g_2 + g_3 = 0.$$

Equations (3.5) and (3.6) correspond to orthogonality of scaling functions. Equation 3.7 shows the dilation property.

Detailed study of Daubechies filters can be found in [3].

#### 3.2.1.1 Daubechies Scaling and Wavelet Functions

In this subsection, we only give an example of filters construction for the Db2 scaling function, based on the computation of its values on integers, and then on dyadic grids. For the general case of construction based on the Fourier transform of the wavelet functions and its properties, see [3]. In [2] one can find how to compute these values of  $\varphi$  at all dyadic points  $x = \frac{l}{2^n}$ . This procedure can be seen in the following steps.

##### Step 1. compute $\varphi$ at all the integer values

In the case of **Db2**, the *scaling function* is nonzero only on the interval  $0 < x < 3$ . So  $\varphi(0) = \varphi(3) = 0$ .  $\varphi(1)$  and  $\varphi(2)$  are the only two nonzero values at integer points, Figure 1. So for  $x = 1$  and  $x = 2$ , the scaling equation

$$\varphi(x) = \sum_k h_k \varphi(2x - k),$$

implies that

$$\varphi(1) = h_0 \varphi(2) + h_1 \varphi(1),$$

and

$$\varphi(2) = h_2 \varphi(2) + h_3 \varphi(1).$$

So

$$(h_1 - 1)\varphi(1) + h_0\varphi(2) = 0, \quad (3.8)$$

on the other hand, to arrange the normalization  $\int \varphi = 1$ , we need  $\sum_l \varphi(l) = 1$ . Hence

$$\varphi(1) + \varphi(2) = 1. \quad (3.9)$$

Thus the solution of equations (3.8) and (3.9) in the case of the **Db2** are

$$\varphi(1) = \frac{1 + \sqrt{3}}{2},$$

and

$$\varphi(2) = \frac{1 - \sqrt{3}}{2}.$$

### Step 2. Compute $\varphi$ at the half integers

In the case of **Db2**, we know  $\varphi(x) = 0$  for  $x \leq 0$  and  $x \geq 3$ . So we need only to compute  $\varphi(\frac{l}{2})$  for  $l = 1, 3, 5$ . For  $x = \frac{l}{2}$  using the scaling equation,

$$\varphi\left(\frac{l}{2}\right) = \sum_k h_k \varphi(l - k),$$

implies that

$$\varphi\left(\frac{1}{2}\right) = h_0\varphi(1) = \frac{(1 + \sqrt{3})^2}{8},$$

$$\varphi\left(\frac{3}{2}\right) = h_1\varphi(2) + h_2\varphi(1) = 0,$$

$$\varphi\left(\frac{5}{2}\right) = h_2\varphi(3) = \frac{(-1 + \sqrt{3})^2}{8}.$$

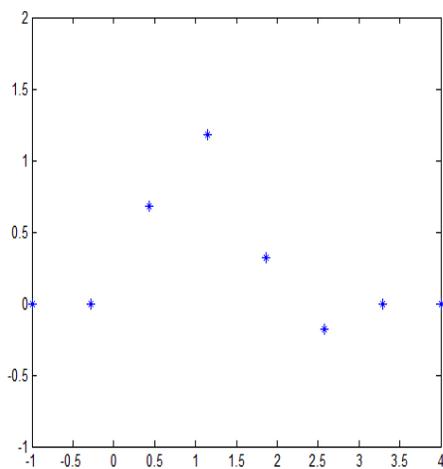
### Step 3. Iterate

By continuing this procedure, computing values of  $\varphi$  at  $\frac{l}{4}$  is similar, we just consider  $x = \frac{l}{4}$  in the scaling equation. In general, computing  $\varphi$  at the values  $x = \frac{l}{2^{n-1}}$ , leads to compute the value of  $\varphi$  at  $x = \frac{l}{2^n}$ . Now we are able to compute the *wavelet function*  $\psi$  using the scaling function  $\varphi$  as

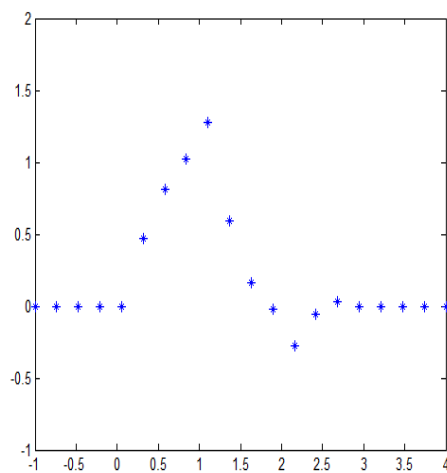
$$\psi(x) = \sum_{k \in \mathbb{Z}} (-1)^k h_{1-k} \varphi(2x - k).$$

Figure 1 shows the graphs of scaling function  $\varphi$  that results from 1 to 4 iterations, and Figure 2 depicts 1 to 4 iterations of this procedure for wavelet function  $\psi$ .

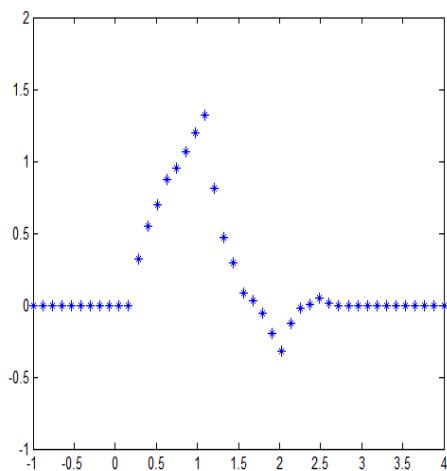
### Scaling Function Construction via Cascade Algorithm Iterations



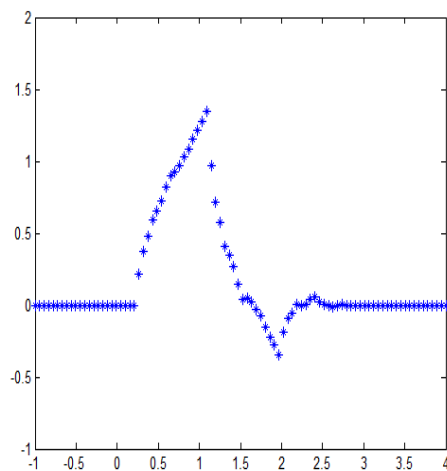
(a) Db2 scaling function in first level iteration



(b) Db2 scaling function in second level iteration



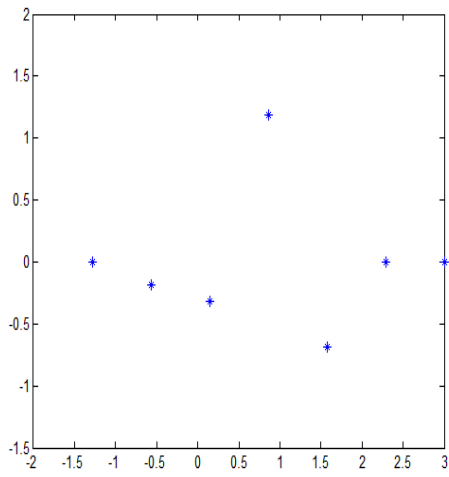
(c) Db2 scaling function in third level iteration



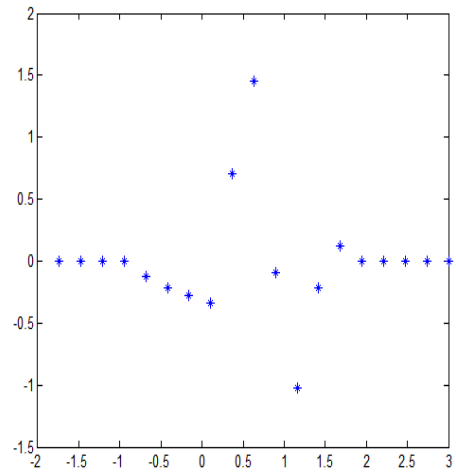
(d) Db2 scaling function in fourth level iteration

Figure 1: Db2 scaling function  $\varphi$  that results from iterating the procedure 1 to 4 times.

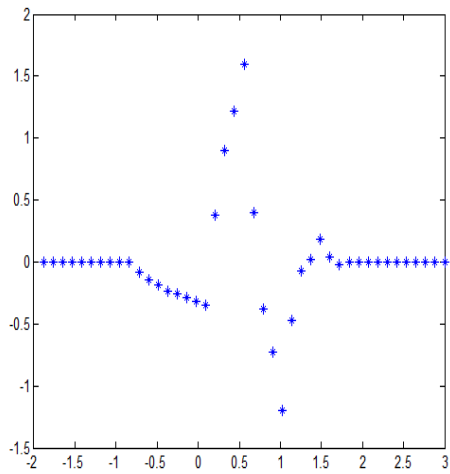
### Wavelet Function Construction via Cascade Algorithm Iterations



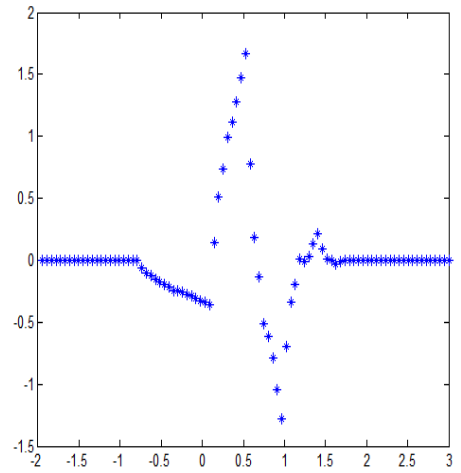
(a) Db2 wavelet function in first level iteration



(b) Db2 wavelet function in first level iteration



(c) Db2 wavelet function in first level iteration



(d) Db2 wavelet function in first level iteration

Figure 2: Db2 wavelet function  $\psi$  that results from iterating the procedure 1 to 4 times.

### 3.2.2 Haar Wavelet Transform

The Haar functions were first defined by Alfred Haar in 1909, and they were recognized by Ingrid Daubechies as being also an example of orthonormal wavelet functions with compact support. Haar used these functions as an example of orthonormal system for the square integrable functions. Haar wavelet transform is a simple example of Daubechies family with 2 scaling filters coefficients which is denoted by  $Db1$ .

#### Definition 3.1. Haar Scaling and Wavelet Functions

Haar scaling and wavelet functions are defined as

$$\varphi(x) = \begin{cases} 1 & 0 \leq x \leq 1 \\ 0 & \text{otherwise} \end{cases}, \psi(x) = \begin{cases} 1 & 0 \leq x \leq 1/2 \\ -1 & 1/2 \leq x \leq 1 \\ 0 & \text{otherwise.} \end{cases} \quad (3.10)$$

Figure 3 depicts the graphs of Haar scaling and wavelet functions.

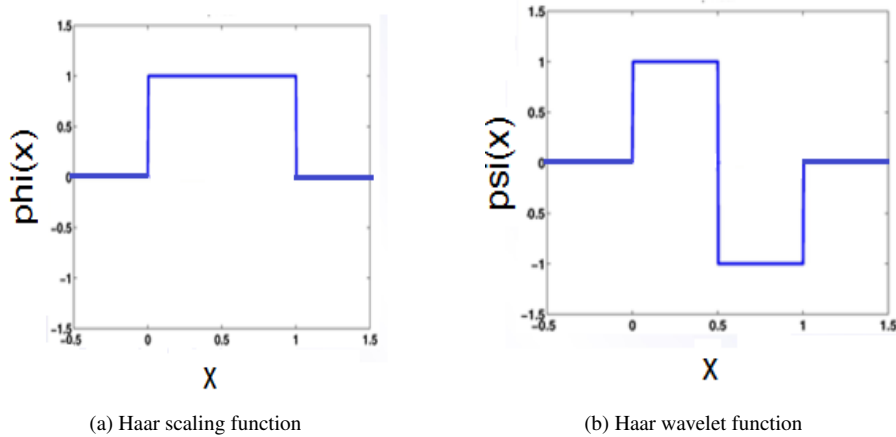


Figure 3: Haar scaling and wavelet functions

We can obtain the function  $\varphi(x - k)$  with the graph of  $\varphi(x)$  by translating  $k$  units to the right. It is obvious that  $\varphi(x - k)$  is discontinuous at  $x = k$  and  $x = k + 1$ . In general, we can define a family of shifted and translated scaling functions  $\{\varphi_{j,k}(x)\}_{j,k \in \mathbb{Z}}$  by:

$$\varphi_{j,k}(x) = 2^{j/2} \varphi(2^j x - k).$$

Recalling the definition 3.1, we may write the following equation

$$\varphi(2^j x - k) = \begin{cases} 1 & k2^{-j} \leq x < (k+1)2^{-j} \\ 0 & \text{otherwise.} \end{cases}$$

The set  $\{2^{\frac{j}{2}}\varphi(2^jx - k)\}_{j,k \in \mathbb{Z}}$  is an orthonormal basis for  $V_j$ . In order to decompose a function properly, we need to decompose  $V_j$  as an orthogonal sum of  $V_{j-1}$  and the space of its complement. So to define this orthogonal space, we need to define a translate and dilate function  $\psi$ . Hence the main tool to construct  $\psi \in V_1$  is that it should be orthogonal to  $V_0$ , it means that for all  $k \in \mathbb{Z}$ ,

$$\int_{-\infty}^{+\infty} \psi(x)\varphi(x-k)dx = 0.$$

According to [1], Haar scaling filter coefficients are obtained as:

$$h_k = \sqrt{2} \int \varphi(x)\varphi(2x-k)dx = \begin{cases} \frac{1}{\sqrt{2}} & \text{if } k = 0, 1 \\ 0 & \text{otherwise.} \end{cases} \quad (3.11)$$

So wavelet filter coefficients  $g_k = (-1)^k h_{1-k}$  are calculated as

$$g_k = \begin{cases} \frac{1}{\sqrt{2}} & \text{for } k = 0 \\ -\frac{1}{\sqrt{2}} & \text{for } k = 1 \\ 0 & \text{otherwise.} \end{cases} \quad (3.12)$$

Since Haar function is a good example which satisfies multiresolution analysis properties, we can use it to approximate functions at different levels of resolution [15].

By definition 3.1,  $f_j$  is piecewise constant on the interval  $(\frac{k}{2^j}, \frac{k+1}{2^j})$ . In [1], the scaling values  $c_{j,k}$  are calculated as

$$c_{j,k} = \frac{1}{\sqrt{2}}(c_{j+1,2k} + c_{j+1,2k+1}).$$

Also the wavelet values (coefficients)  $d_{j,k}$  at scale  $j$  are obtained as

$$d_{j,k} = \frac{1}{\sqrt{2}}(c_{j-1,2k} - c_{j-1,2k+1}).$$

This means that, we measure the derivation of  $f_j$  from its mean value on the interval  $(\frac{k}{2^j}, \frac{k+1}{2^j})$ . Hence in order to obtain the *decomposition* of  $f_j$ , we continue this procedure.

### 3.2.3 Cascade Algorithm

One type of fast approach to compute the normalized discrete wavelet transform is decimated algorithms, in which each time a new decomposition levels is calculated, the input discrete data (vector) is divided into two other vectors with half of the size of the original one. since these algorithms apply the same procedure over and over to the output of the previous sampling points, it is known as the *cascade algorithm*.

Consider the function  $f$  with  $N$  samples, where  $N = 2^L$ . The following algorithm describes the cascade algorithm in order to decompose  $f$  into different frequency domain. Here we use the same notation for scaling and wavelet coefficients. According

to the definition (3.3), we come up with the conclusion that the level of decomposition is related to the number of samples of discrete data, for example, a function with  $8 = 2^3$  samples can be decomposed to 3 levels (the final level).

---

**Algorithm 1** Decomposition

---

```

for  $j = 1 \rightarrow L$  do
  for  $k = 0 \rightarrow 2^{L-j} - 1$  do
    for  $l = 0 \rightarrow D - 1$  do
       $c_{j,k} = \frac{1}{\sqrt{2}} \sum_l h_l c_{j-1,2k+l}$ 
       $d_{j,k} = \frac{1}{\sqrt{2}} \sum_l g_l c_{j-1,2k+l}$ 
    end for
  end for
end for

```

---



---

**Algorithm 2** Reconstruction

---

```

for  $j = L - 1 \rightarrow 0$  do
  for  $k = 0 \rightarrow 2^{L-j} - 1$  do
    for  $l = 0 \rightarrow D - 1$  do
       $c_{j,k} = \frac{1}{\sqrt{2}} (\sum_l h_l c_{j+1,k+2l} + \sum_l g_l d_{j+1,k+2l})$ 
    end for
  end for
end for

```

---

### 3.2.4 Boundary problem

In the case of Daubechies wavelet decomposition with 4 filters or more, cascade algorithm faces a problem on the boundaries, since for the last positions of any level of decomposition, the fixed sized filters will need to access data no longer inside the vector with the signal samples. It means that, we always require unknown samples to construct the last scaling and wavelet coefficients. The number of run out values depends on the length of the wavelet filters. So by considering the specific wavelet transform, we can extend the given sample beyond the initial set of data.

According to [2], to circumvent this problem, and handle boundaries with extended data, we tested some well established methods called Periodic, Zero, and Symmetric extensions as describe below.

#### 1. Periodic Extension

Here, we perform an even extension by  $f_{n+k} = f_k$ , and make the function *periodic*. It means that, we repeat the values of samples all over again.

For better understanding, consider a function  $f$  with 8 samples  $(f_1, f_2, \dots, f_8)$  and decompose it with **Db2** wavelet transform. In the first level of decomposition, we need

to extend  $f$  in order to be able to compute the last scaling and wavelet coefficients  $s_4$  and  $d_4$ . Then we construct a function  $\tilde{f}$  which is the *periodic extension* of the function  $f$  where  $f_9 = f_1$  and  $f_{10} = f_2$ .

$$\tilde{f} = (f_1, f_2, \dots, f_8, f_9, f_{10}).$$

Now we are able to pass function  $f \in V_1$  through the scaling ( $h$ ) and wavelet ( $g$ ) filters in order to get the scaling  $s \in V_0$  and wavelet  $d \in W_0$  coefficients.

The following equation shows how these coefficients are calculated by cascade algorithm:

$$\begin{bmatrix} s_1 \\ s_2 \\ s_3 \\ s_4 \\ d_1 \\ d_2 \\ d_3 \\ d_4 \end{bmatrix} = \begin{bmatrix} h_1 f_1 + h_2 f_2 + h_3 f_3 + h_4 f_4 \\ h_1 f_3 + h_2 f_4 + h_3 f_5 + h_4 f_6 \\ h_1 f_5 + h_2 f_6 + h_3 f_7 + h_4 f_8 \\ h_1 f_7 + h_2 f_8 + h_3 f_1 + h_4 f_2 \\ g_1 f_1 + g_2 f_2 + g_3 f_3 + g_4 f_4 \\ g_1 f_3 + g_2 f_4 + g_3 f_5 + g_4 f_6 \\ g_1 f_5 + g_2 f_6 + g_3 f_7 + g_4 f_8 \\ g_1 f_7 + g_2 f_8 + g_3 f_1 + g_4 f_2 \end{bmatrix}.$$

Hence the first level transformed matrix is:

$$T_p = \begin{bmatrix} h_1 & h_2 & h_3 & h_4 & 0 & 0 & 0 & 0 \\ 0 & 0 & h_1 & h_2 & h_3 & h_4 & 0 & 0 \\ 0 & 0 & 0 & 0 & h_1 & h_2 & h_3 & h_4 \\ h_3 & h_4 & 0 & 0 & 0 & 0 & h_1 & h_2 \\ - & - & - & - & - & - & - & - \\ g_1 & g_2 & g_3 & g_4 & 0 & 0 & 0 & 0 \\ 0 & 0 & g_1 & g_2 & g_3 & g_4 & 0 & 0 \\ 0 & 0 & 0 & 0 & g_1 & g_2 & g_3 & g_4 \\ g_3 & g_4 & 0 & 0 & 0 & 0 & g_1 & g_2 \end{bmatrix}.$$

This method shows that in transformed matrix, coefficients  $h$  and  $g$  which are annihilated on the left reappear on the right. It means that in each step, the  $h$  and  $g$  coefficients are moved to the right by 2 steps (cascade algorithm), and the first pair of positions in the last step are filled in periodically.

By the properties of **D<sub>b</sub>2** filters we know that

$$h_1^2 + h_2^2 + h_3^2 + h_4^2 = 1, \quad h_1 h_3 + h_2 h_4 = 0,$$

and

$$g_1^2 + g_2^2 + g_3^2 + g_4^2 = 1, \quad g_1 g_3 + g_2 g_4 = 0,$$

so we have

$$T_p T_p^T = I_8,$$

hence, the periodic extension yields an orthogonal transformed matrix, and the matrix

$T_p^{-1}$  describe below is used to reconstruct the function  $f$  in **Db2** periodic system.

$$T_p^{-1} = \begin{bmatrix} h_1 & 0 & 0 & h_3 & g_1 & 0 & 0 & g_3 \\ h_2 & 0 & 0 & h_4 & g_2 & 0 & 0 & g_4 \\ h_3 & h_1 & 0 & 0 & g_3 & g_1 & 0 & 0 \\ h_4 & h_2 & 0 & 0 & g_4 & g_2 & 0 & 0 \\ 0 & h_3 & h_1 & 0 & 0 & g_3 & g_1 & 0 \\ 0 & h_4 & h_2 & 0 & 0 & g_4 & g_2 & 0 \\ 0 & 0 & h_3 & h_1 & 0 & 0 & g_3 & g_1 \\ 0 & 0 & h_4 & h_2 & 0 & 0 & g_4 & g_2 \end{bmatrix}.$$

## 2. Zero Padding Extension

Another approach to tackle the overlap issue is to add enough zeros to the initial function  $f$ , ( $f_k = 0$  for  $k < 0$  and  $k > n - 1$ ).

In order to decompose function  $f$  with 8 samples in **Db2** wavelet system, we should extend it by  $\tilde{f}$  where the values  $f_9 = f_{10}$  set to zero.

$$\tilde{f} = (f_1, f_2, \dots, f_8, 0, 0).$$

For  $f \in V_1$ , the coefficients  $s$  and  $d$  in scaling and wavelet spaces  $V_0$  and  $W_0$  are obtained as:

$$\begin{bmatrix} s_1 \\ s_2 \\ s_3 \\ s_4 \\ d_1 \\ d_2 \\ d_3 \\ d_4 \end{bmatrix} = \begin{bmatrix} h_1 f_1 + h_2 f_2 + h_3 f_3 + h_4 f_4 \\ h_1 f_3 + h_2 f_4 + h_3 f_5 + h_4 f_6 \\ h_1 f_5 + h_2 f_6 + h_3 f_7 + h_4 f_8 \\ h_1 f_7 + h_2 f_8 \\ g_1 f_1 + g_2 f_2 + g_3 f_3 + g_4 f_4 \\ g_1 f_3 + g_2 f_4 + g_3 f_5 + g_4 f_6 \\ g_1 f_5 + g_2 f_6 + g_3 f_7 + g_4 f_8 \\ g_1 f_7 + g_2 f_8 \end{bmatrix}.$$

So the first level transformed matrix  $T_z$  for *zero padding extension* is :

$$T_z = \begin{bmatrix} h_1 & h_2 & h_3 & h_4 & 0 & 0 & 0 & 0 \\ 0 & 0 & h_1 & h_2 & h_3 & h_4 & 0 & 0 \\ 0 & 0 & 0 & 0 & h_1 & h_2 & h_3 & h_4 \\ 0 & 0 & 0 & 0 & 0 & 0 & h_1 & h_2 \\ - & - & - & - & - & - & - & - \\ g_1 & g_2 & g_3 & g_4 & 0 & 0 & 0 & 0 \\ 0 & 0 & g_1 & g_2 & g_3 & g_4 & 0 & 0 \\ 0 & 0 & 0 & 0 & g_1 & g_2 & g_3 & g_4 \\ 0 & 0 & 0 & 0 & 0 & 0 & g_1 & g_2 \end{bmatrix}.$$

The main difference between transformed matrices  $T_p$  and  $T_z$  is orthogonality. The matrix  $T_z$  is not orthonormal. since the first pair of positions in the last step in  $T_z$  are filled by zero, further we will see that reconstruction by zero padding method does not give us the initial data. In this case we can calculate the error.

Suppose that the function  $\hat{f} = (\hat{f}_1, \hat{f}_2, \dots, \hat{f}_N)$  is the reconstruction of the function  $f$  with  $N$  samples by **Db2** zero padding transform. Then the  $l^2$ -norm error is calculated as:

$$\|f - \hat{f}\|_{l_2} = \frac{1}{N} \left( \sum_{k=1}^N (f_k - \hat{f}_k)^2 \right)^{\frac{1}{2}}.$$

### 3. Symmetric Extension

The third approach to deal with boundaries is *symmetric extension*.

In this method, the function is extended at the end points by reflection, (they are mirrored at end points).

To decompose a function  $f$  with 8 samples in **Db2** wavelet system, we need to extend it by  $\tilde{f}$  where values  $f_9 = f_8$  and  $f_{10} = f_7$ .

$$\tilde{f} = (f_1, f_2, \dots, f_8, f_8, f_7).$$

For  $f \in V_1$ , the coefficients  $s$  and  $d$  in scaling and wavelet spaces  $V_0$  and  $W_0$  are obtained as:

$$\begin{bmatrix} c_1 \\ c_2 \\ c_3 \\ c_4 \\ d_1 \\ d_2 \\ d_3 \\ d_4 \end{bmatrix} = \begin{bmatrix} h_1 f_1 + h_2 f_2 + h_3 f_3 + h_4 f_4 \\ h_1 f_3 + h_2 f_4 + h_3 f_5 + h_4 f_6 \\ h_1 f_5 + h_2 f_6 + h_3 f_7 + h_4 f_8 \\ (h_1 + h_4) f_7 + (h_2 + h_3) f_8 \\ g_1 f_{1,1} + g_2 f_2 + g_3 f_3 + g_4 f_4 \\ g_1 f_{1,3} + g_2 f_4 + g_3 f_5 + g_4 f_6 \\ g_1 f_{1,5} + g_2 f_6 + g_3 f_7 + g_4 f_8 \\ (g_1 + g_4) f_7 + (g_2 + g_3) f_8 \end{bmatrix}.$$

So the first level transformed matrix  $T_s$  is

$$T_s = \begin{bmatrix} h_1 & h_2 & h_3 & h_4 & 0 & 0 & 0 & 0 \\ 0 & 0 & h_1 & h_2 & h_3 & h_4 & 0 & 0 \\ 0 & 0 & 0 & 0 & h_1 & h_2 & h_3 & h_4 \\ 0 & 0 & 0 & 0 & 0 & 0 & h_1 + h_4 & h_2 + h_3 \\ - & - & - & - & - & - & - & - \\ g_1 & g_2 & g_3 & g_4 & 0 & 0 & 0 & 0 \\ 0 & 0 & g_1 & g_2 & g_3 & g_4 & 0 & 0 \\ 0 & 0 & 0 & 0 & g_1 & g_2 & g_3 & g_4 \\ 0 & 0 & 0 & 0 & 0 & 0 & g_1 + g_4 & g_2 + g_3 \end{bmatrix}.$$

This matrix is not orthonormal, and the first pair of positions in the last step are filled by zero. The main difference between  $T_s$  and  $T_z$  is the last pair of positions in the last step, which are filled by the combination of filter coefficients.

### Example 3.1. Db2 Decomposition and Reconstruction

Consider the function  $f(x) = \sin(x)$  for  $x = 0 : 2^{10}$ , it means that we have 1024 samples to pass through the filters in order to decompose and reconstruct  $f$ .

The main goal of this example is to decompose and reconstruct this function with all three extension methods and compare the results. For function  $f$  with  $2^{10}$  samples, we are able to do the **decomposition** process up to 10 levels. Consider periodic extension of this function, and perform some level decomposition.

Figure 4 illustrates the scaling and wavelet coefficients for 5 level of decomposition with periodic extension. By increasing the level of iteration, the value of wavelet coefficients decrease, and the effect of the wrapping around the data is visible in wavelet coefficients.

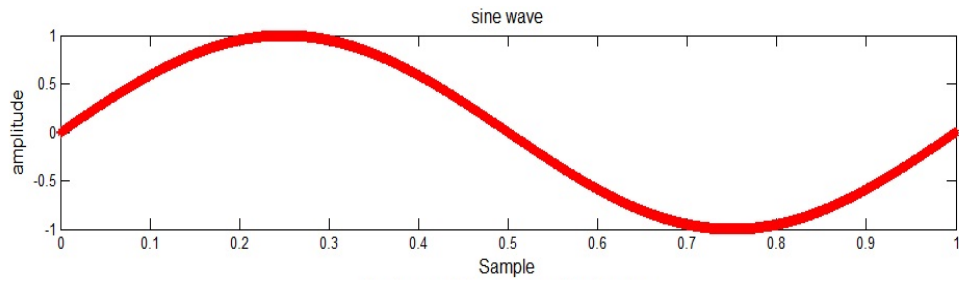
It means that in each level of decomposition, the last two values of wavelet coefficients are not in the same linearity, and they are zero wherever wrapping act is not considered. Now suppose that the right boundary of the function  $f$  is extended with zero padding method. When we do the decomposition, we realize the differences between this extension and the periodic method near boundaries.

Figure 5b shows 5 level wavelet and scaling coefficients, which in comparison with periodic extension, wavelet coefficients are greater and the distortion in the right boundary are more visible. The same distortion in the right boundary happens for symmetric extension.

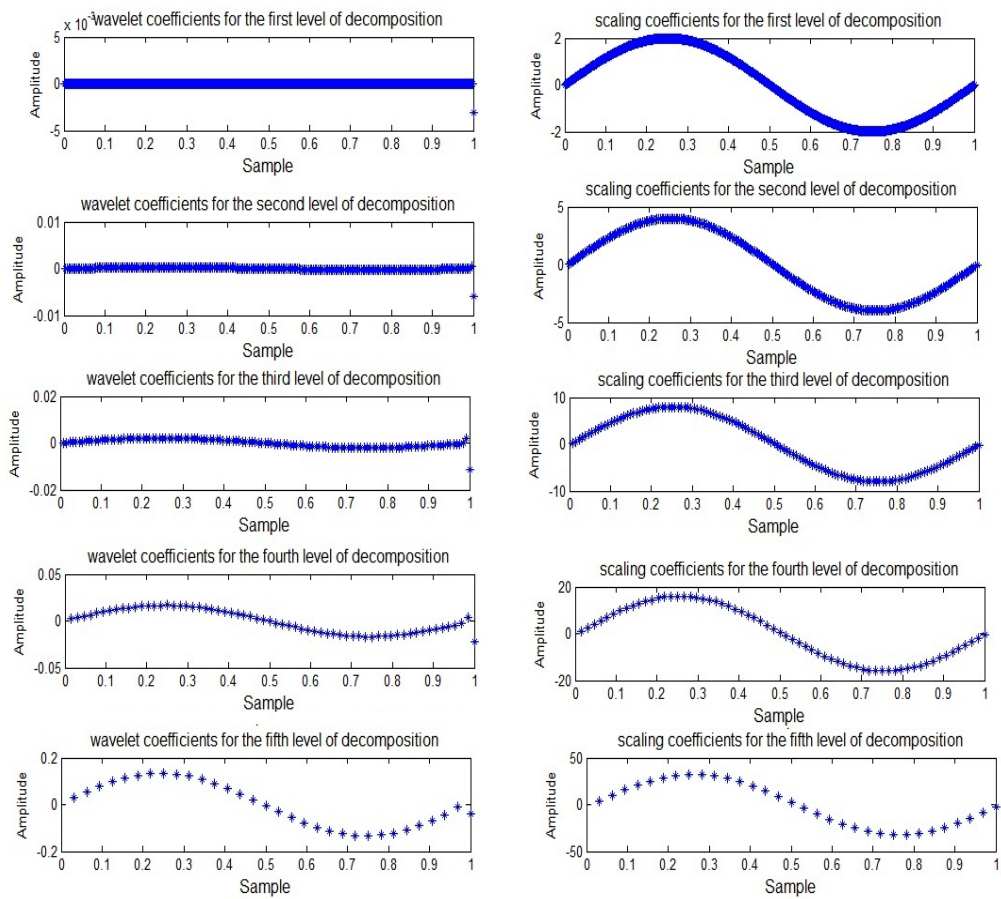
Figure 6b depicts the graph of wavelet and scaling coefficients for function  $f$  in Db2 system with symmetric extension.

Since the initial function  $\sin(x)$  is periodic, comparing these three methods indicates that the periodic extension can be the best way to deal with borders. While, according to the definition of function  $\sin(x)$  in the interval  $[0, 1]$ , we obtain inverse results. Therefore in order to have a periodic function, we should consider  $\sin(x)$  for  $0 \leq x < 1$ .

As we described above, the periodic extension is a suitable method to **reconstruct** periodic functions. It means that we can reconstruct the decomposition function in level  $j$  and return exactly to the initial function (perfect reconstruction) since the periodic extension yields an orthogonal transformed matrix. However, in the zero padding and symmetric extensions, some points in boundaries are not reconstructed perfectly.

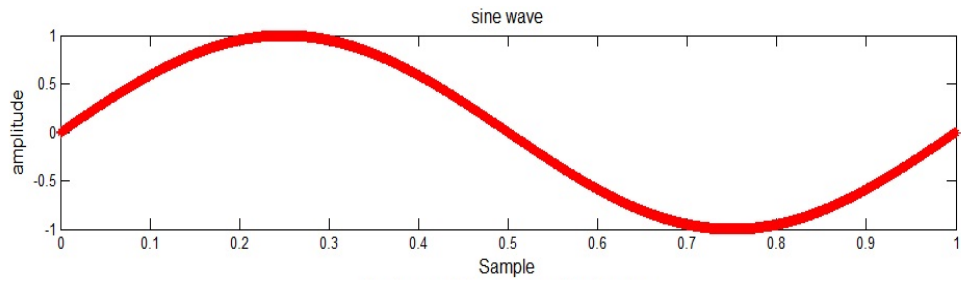


(a)

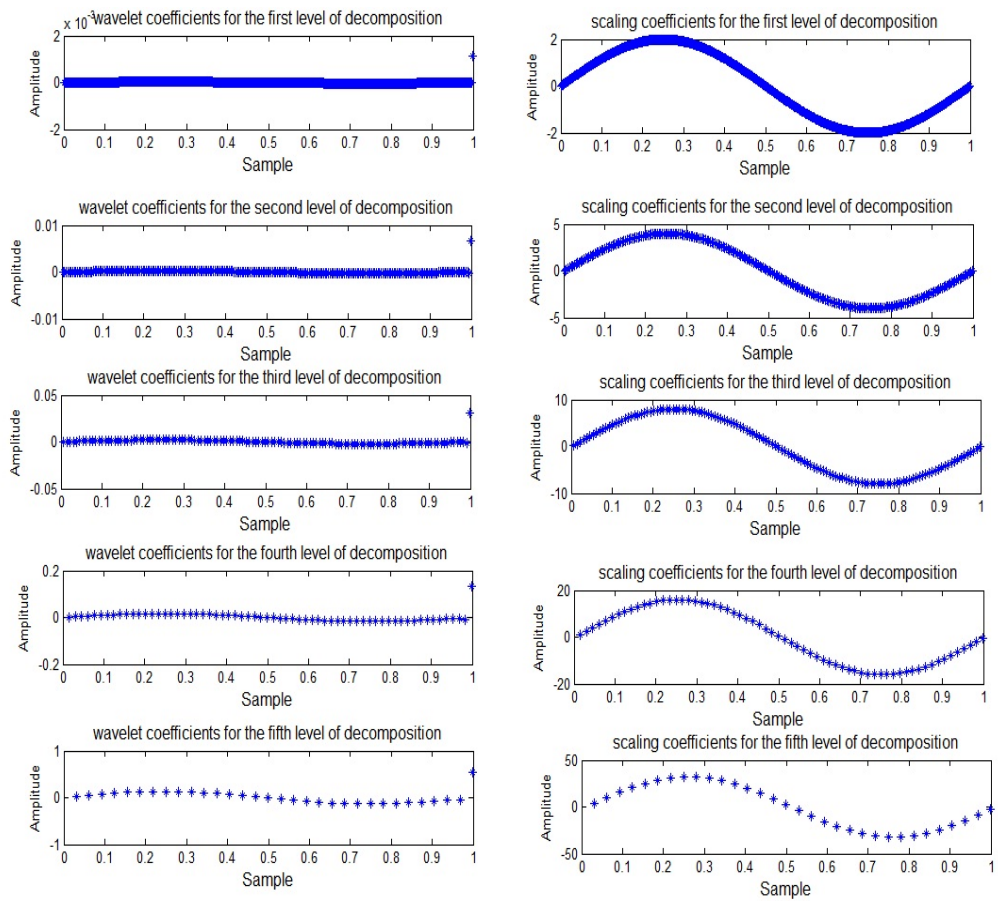


(b)

Figure 4: (a) Depicts the sin function defined in Example 3.1. (b) From up to bottom: 5 level wavelet and scaling coefficients considering Periodic extension for the wavelet transform.

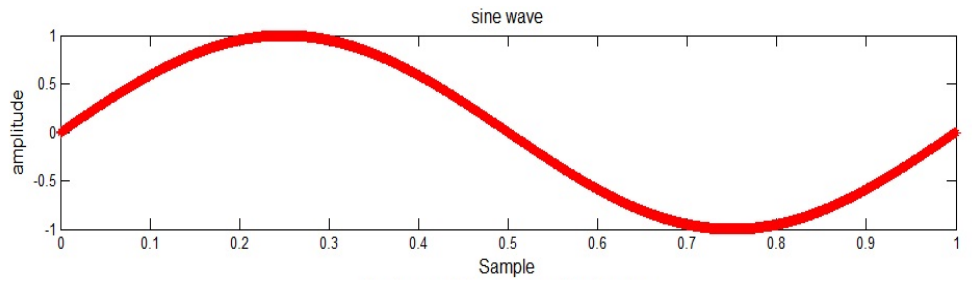


(a)

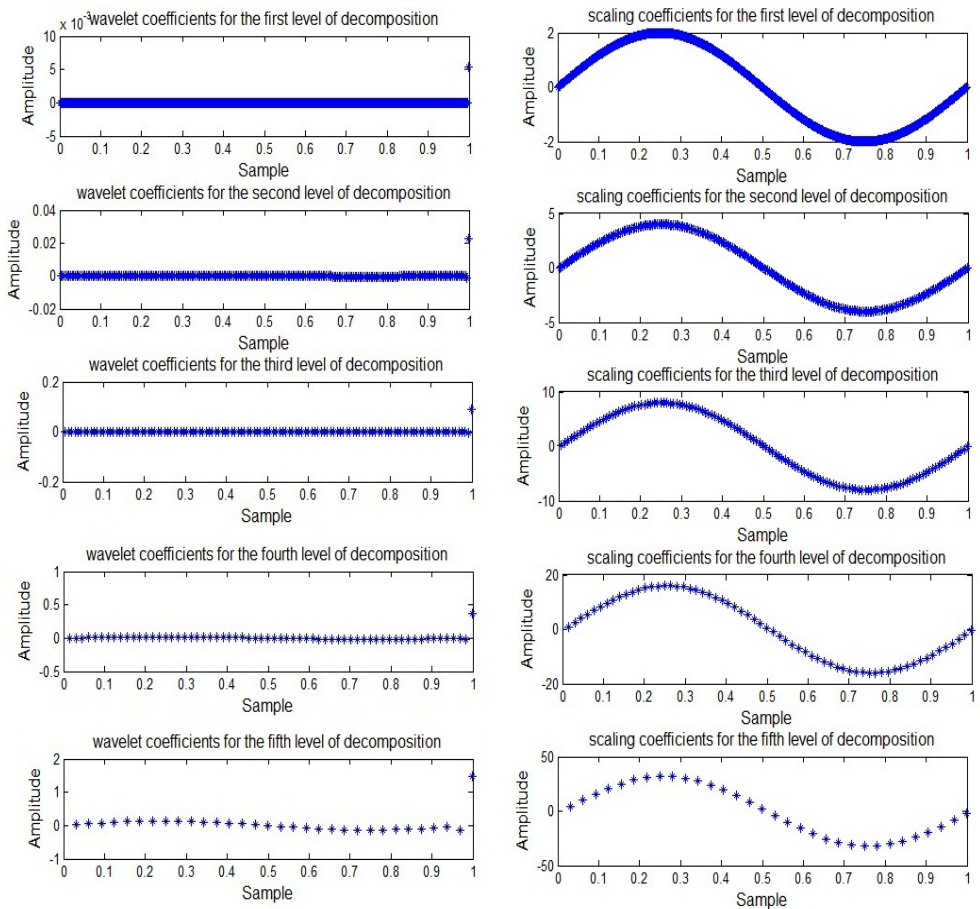


(b)

Figure 5: (a) Depicts the sin function defined in Example 3.1. (b) From up to bottom: 5 level wavelet and scaling coefficients considering Zero padding extension for the wavelet transform.



(a)



(b)

Figure 6: (a) Depicts the sin function defined in Example 3.1. (b) From top to bottom: 5 level wavelet and scaling coefficients considering Symmetric extension for the wavelet transform.

### Example 3.2.

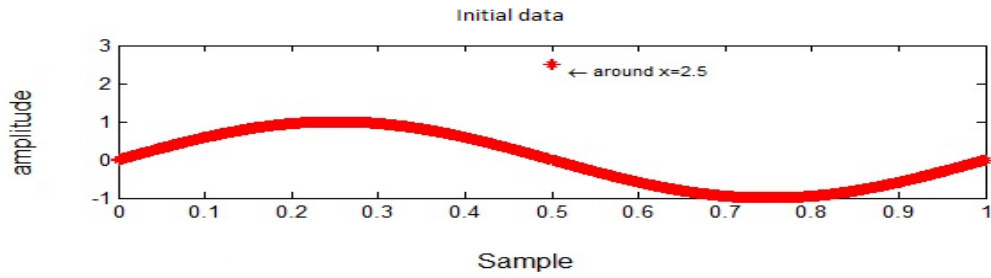
Consider function  $f(x) = \sin(x)$  for  $x = 0 : 2^{10}$ , with three jumps around  $x = 2.5$ . It means that the function  $f$  is continuous and differentiable everywhere except at  $k = \frac{512}{1024}, \frac{513}{1024}, \frac{514}{1024}$ , where  $k$  is the translation number. In this way first level decomposition with any extension (by Db2 wavelet) gives some spikes at the location  $k = \frac{256}{1024}, \frac{257}{1024}, \frac{258}{1024}$  in wavelet and scaling coefficients, where these locations are related to the discontinuity in initial function at perturbation points. It means that the only nonzero wavelet coefficients are near points where the slope changes.

Figure 7 depicts wavelet coefficients in 5 level Db2 decomposition with **periodic** extension. By changing the number of  $k$ , the location of the wavelet coefficients will change along the horizontal axis. As it is expected, in the first level of decomposition the wavelet coefficients correspond to projection of 512 scaling coefficients to the space  $W_0$ .

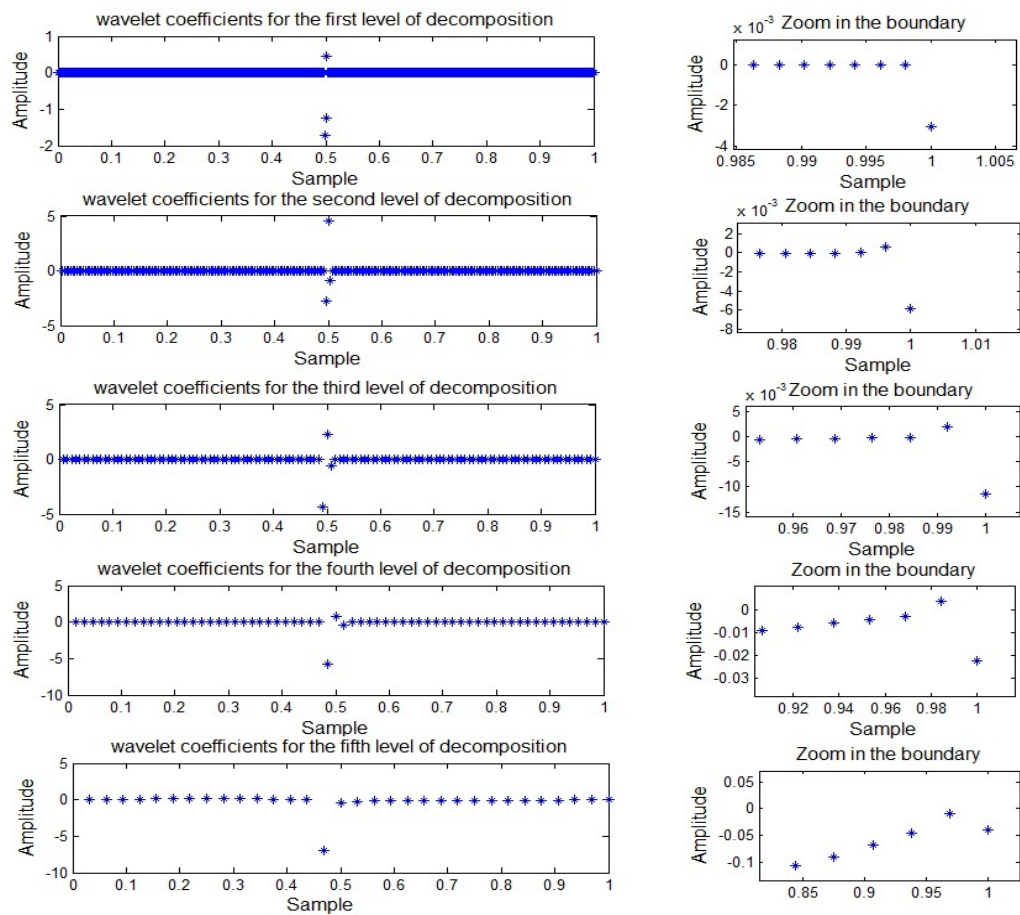
In general, for number of  $N$  sample, the jumps in wavelet coefficients occur at  $k = \frac{2^{N-j-1}}{2^N}, \frac{2^{N-j-1}+1}{2^N}, \frac{2^{N-j-1}+2}{2^N}$ . It means that each coefficient reflects the behavior of a function over a specific time interval, so the coefficients should capture interesting behavior such as sharp changes or smoothness of a function.

Figure 8b and Figure 9b illustrate the wavelet coefficients in 5 level Db2 decompositions by **zero padding** and **symmetric** extension for function Sine with 3 perturbation in the middle.

Looking precisely at all wavelet coefficients in following graphs, we come up to the conclusion that there is no difference in the discontinuity points for all three methods in Db2, and the perturbations in the middle of functions do not affect the scales of the wavelet coefficients in boundaries. The only visible difference between these methods is in right boundaries (as we expected), since the extensions are added in the right boundary.

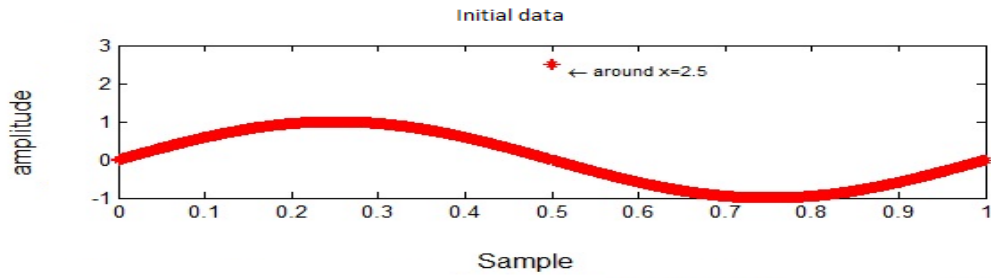


(a)

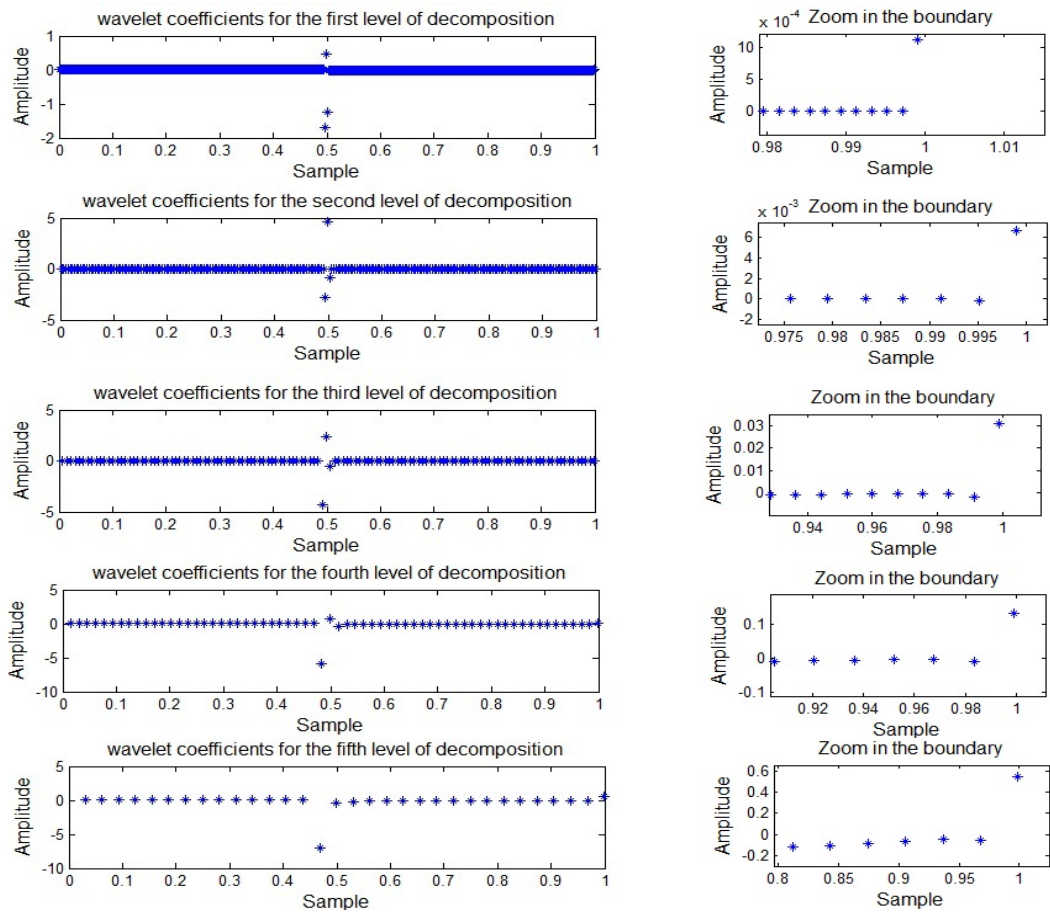


(b)

Figure 7: (a) Depicts sin function with perturbation defined in Example 3.2 . (b) From top to bottom: 5 level wavelet coefficients considering Periodic extension for the wavelet transform, right side panels illustrating boundary effects caused by the chosen extension.

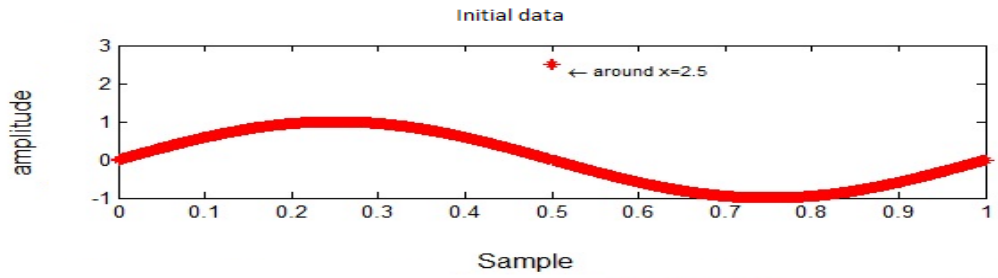


(a)

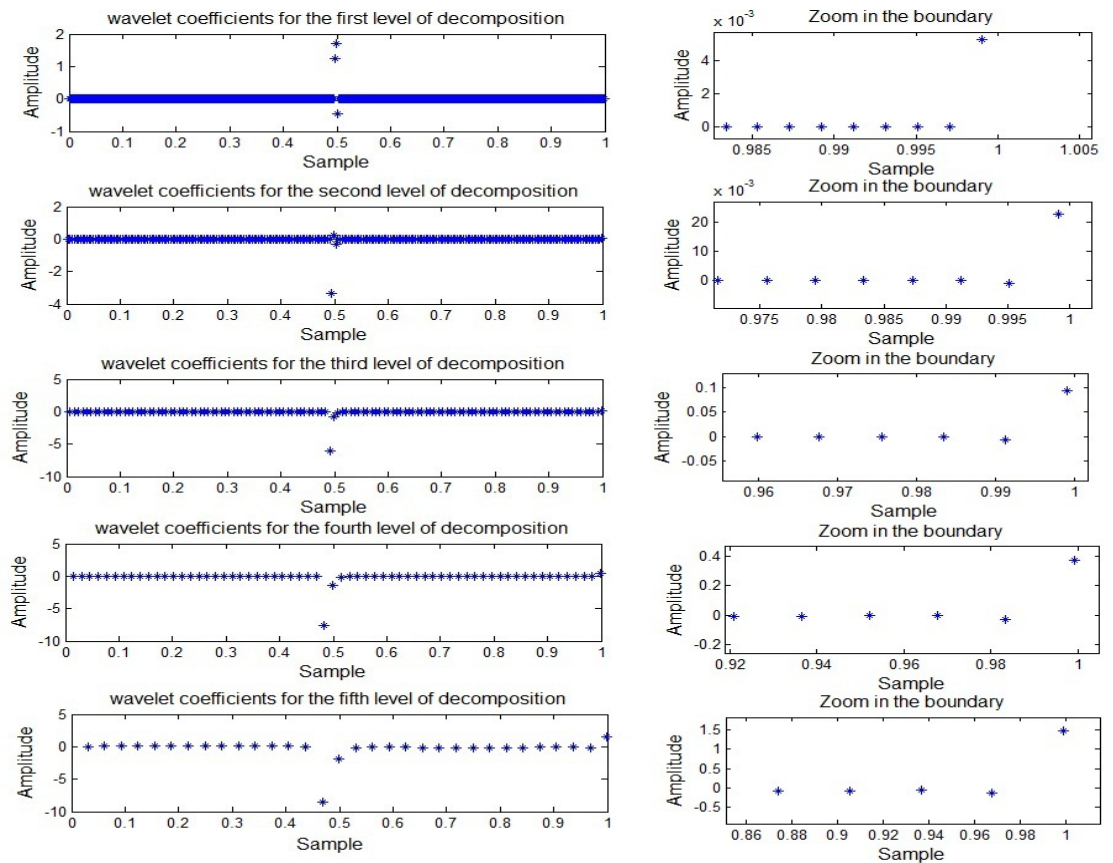


(b)

Figure 8: (a) Depicts sin function with perturbation defined in Example 3.2 . (b) From top to bottom: 5 level wavelet coefficients considering Zero padding extension for the wavelet transform, right side panels illustrating boundary effects caused by the chosen extension.



(a)



(b)

Figure 9: (a) Depicts sin function with perturbation defined in Example 3.2 . (b) From top to bottom: 5 level wavelet coefficients considering Symmetric extension for the wavelet transform, right side panels illustrating boundary effects caused by the chosen extension.

## 4 Two Dimensional Discrete Wavelet System

In section 3 we explained one dimensional discrete wavelet transform based on multiresolution analysis. We applied two different examples and calculated the scaling and wavelet coefficients in different levels by considering Db2 wavelet transform. In order to use wavelets for image processing we need to extend the wavelet transform to multi variables functions.

In this section we describe, based on [2] and [1], how to construct a two dimensional wavelet transform from the uni-dimensional one.

### 4.1 Two Dimensional Scaling and Wavelet Functions

To construct the two dimensional wavelet functions from one dimensional scaling function  $\varphi(x)$  and wavelet function  $\psi(x)$ , we define a *scaling function*  $\Phi(x,y)$  by:

$$\Phi(x,y) = \varphi(x)\varphi(y), \quad (4.1)$$

and three two dimensional *wavelet functions* as

$$\Psi^H(x,y) = \varphi(x)\psi(y),$$

$$\Psi^V(x,y) = \psi(x)\varphi(y),$$

$$\Psi^D(x,y) = \psi(x)\psi(y).$$

Dilated, translated, and normalized scaling and wavelet functions are defined by

$$\Phi_{j,k}(x,y) = 2^j \Phi(2^j x - k_x, 2^j y - k_y),$$

$$\Psi_{j,k}^H(x,y) = 2^j \Psi^H(2^j x - k_x, 2^j y - k_y),$$

$$\Psi_{j,k}^V(x,y) = 2^j \Psi^V(2^j x - k_x, 2^j y - k_y),$$

$$\Psi_{j,k}^D(x,y) = 2^j \Psi^D(2^j x - k_x, 2^j y - k_y),$$

where  $j \in \mathbb{Z}$  and  $k \in \mathbb{Z}^2$ .

So the two dimensional subspace  $V_j^2 = V_j \otimes V_j \subset L^2(\mathbb{R}^2)$  at scale  $j$  is spanned by  $\Phi(2^j x - k_x, 2^j y - k_y)$  of the scaling function  $\Phi$ , and it can be defined as the set of all functions of the form

$$f_j(x,y) = \sum_k c_{j,k} \Phi_{j,k}(x,y) = \sum_k c_{j,k} \varphi_{j,k}(x) \varphi_{j,k}(y).$$

In this work we are not going to study continuous functions in  $L^2(\mathbb{R}^2)$ . Instead we are interested in discrete objects represented by matrices, as the mammograms images are analysing in the applications. Therefore we scape the presentation of the MRA in 2 dimensions [1], and focus on the discrete 2 dimansion wavelet transform.

## 4.2 Two Dimensional Wavelet Transform

The construction of the discrete transformation is a consequence of the definition 4.1, since now the  $x$  and  $y$  directions are going to be decomposed in terms of the 1 dimensional wavelet transform.

Lets consider the set of input data represented by the matrix  $M = [f_{n,m}]$  where  $n, m = 0, \dots, N_k - 1$  and  $N_k = 2^{N_{max}}$ .

The 1 level two dimension discrete wavelet transform is defined by first applying 1 dimensional discrete wavelet transform on rows matrix  $M$  (denoted by  $\tilde{M}$ ), and then applying 1 dimensional discrete wavelet transform on columns of resulting matrix  $\tilde{M}$  (denoted by  $\hat{M}$ ).

The result of the first level decomposition process is the matrix with 4 blocks.

$$H_y H_x M_j, \quad H_y G_x M_j, \quad G_y H_x M_j, \quad G_y G_x M_j,$$

where the size of each block is the half size of the function  $M$ .

The block  $H_y H_x M_j$  (left up corner) contains low frequency (smooth) function, it is scaling coefficients block. The right up corner block ( $H_y G_x$ ) contains horizontal high frequency, the left down corner block ( $G_y H_x$ ) has vertical high frequency, and the right down corner block ( $G_y G_x$ ) shows the diagonal pattern. All this three are the wavelet coefficients blocks.

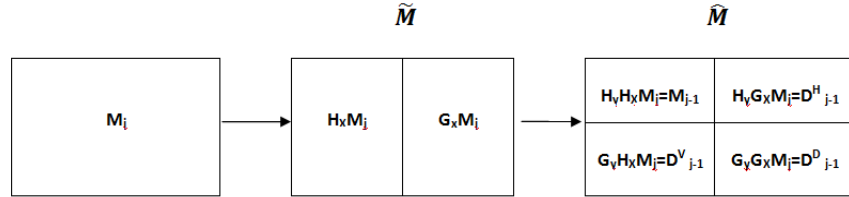
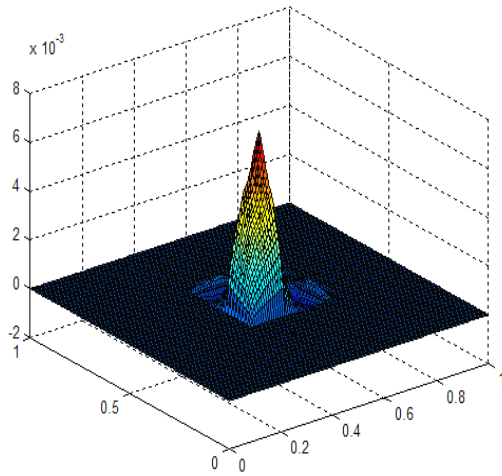


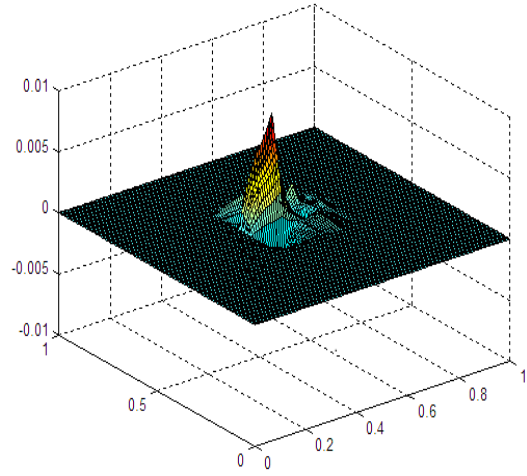
Figure 10: Two dimensional wavelet decomposition. Each  $M_j$  can be decomposed as  $M_j = M_{j-1} + D_{j-1}^H + D_{j-1}^V + D_{j-1}^D$ .

In Figure 11 we present for the Db2 filters the construction of the scaling function and the three corresponding wavelet functions denoted as horizontal, vertical and diagonal wavelets. Each function is obtained by considering a coefficient of corresponded block to one and set other blocks to zero and reconstruct all four blocks ( $M_{j-1}, D_{j-1}^H, D_{j-1}^V, D_{j-1}^D$ ) together, for instance scaling function  $\Phi(x, y)$  represented in figure 11a is obtained from the reconstruction of four blocks where all coefficients except one in up left subband ( $M_{j-1}$ ) are set to zero.

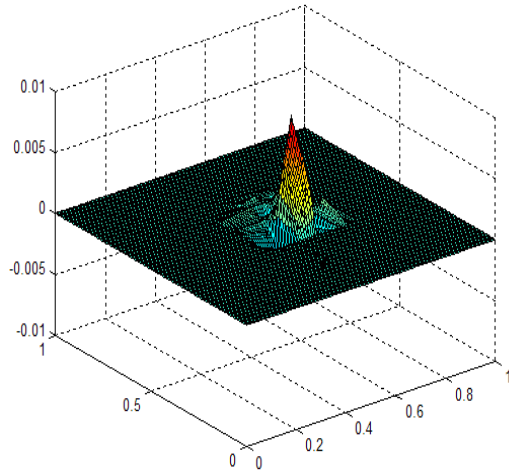
The cascade Algorithm used in this case shows the two dimensional wavelet decomposition for function of the length  $N * N$  where  $N = 2^L$ . where the length of the wavelet filter is considered  $D$ .



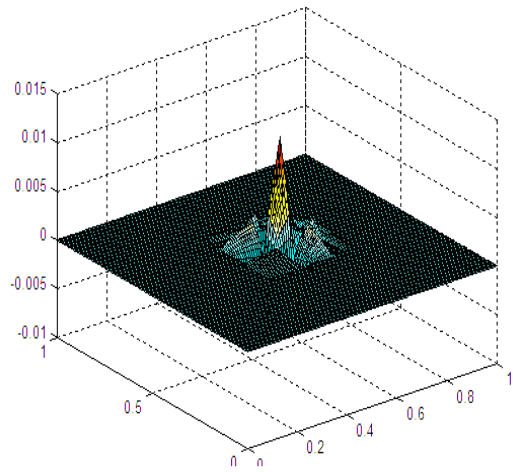
(a) Two dimensional Db2 scaling function  $\Phi(x,y)$



(b) Two dimensional Db2 horizontal wavelet function  $\Psi^H(x,y)$



(c) Two dimensional Db2 vertical wavelet function  $\Psi^V(x,y)$



(d) Two dimensional Db2 diagonal wavelet function  $\Psi^D(x,y)$

Figure 11: (a) Db2 scaling function that is obtained from the reconstruction of the up left block. (b) Db2 horizontal wavelet function which is related to the up right block. (c) Db2 vertical wavelet function which is captured from reconstruction of the down left block. (d) Db2 diagonal wavelet function.

---

**Algorithm 3** Two Dimensional Decomposition
 

---

```

for  $j = 1 \rightarrow L$  do
  for  $k_x = 0 \rightarrow 2^{L-j} - 1$  do
    for  $k_y = 1 \rightarrow 2^{L-j} - 1$  do
      for  $l = 0 \rightarrow D - 1$  do
         $c_{k_x, k_y}^j = \sum_l h_l c_{2k_x+1, 2k_y+l}^{j-1}$ 
         $d_{k_x, k_y}^j = \sum_l g_l c_{2k_x+1, 2k_y+l}^{j-1}$ 
      end for
    end for
  end for
   $c_{k_x, k_y}^j = \sum_l h_l c_{2k_x+1, 2k_y+l}^j$ 
   $d_{k_x, k_y}^h = \sum_l g_l d_{2k_x+1, 2k_y+l}^j$ 
   $d_{k_x, k_y}^v = \sum_l h_l d_{2k_x+1, 2k_y+l}^j$ 
   $d_{k_x, k_y}^d = \sum_l g_l d_{2k_x+1, 2k_y+l}^j$ 
end for

```

---

**Example 4.1. Two Dimensional Db2 Wavelet Transform**

Consider the input matrix  $M = [f_{ij}]$  defined by  $f_{ij} = i * x_j$  where  $x_j = \frac{j}{16}$  for  $i, j = 1, 2, \dots, 16$ , represented by Figure 12. Each line of the input matrix is generated by a linear function discretized in a fine grid with step  $\frac{1}{16}$ .

To decompose the matrix  $M$  with  $16 * 16$  values, we consider two dimensional wavelet transform. since Db2 wavelet transform has filters greater than 2, some data extension has to be performed on the boundaries, exactly as in the one-dimensional case. Here and in the applications we only consider periodic extension because they cause less distortions in the final results.

$$M = \begin{bmatrix} 0.06 & 0.12 & 0.18 & 0.25 & 0.31 & 0.37 & 0.43 & 0.5 & 0.56 & 0.62 & 0.68 & 0.7 & 0.81 & 0.87 & 0.93 & 1 \\ 0.12 & 0.25 & 0.37 & 0.5 & 0.62 & 0.7 & 0.87 & 1 & 1.1 & 1.2 & 1.3 & 1.5 & 1.6 & 1.7 & 1.8 & 2 \\ 0.18 & 0.37 & 0.56 & 0.7 & 0.93 & 1.1 & 1.3 & 1.5 & 1.6 & 1.8 & 2 & 2.2 & 2.4 & 2.6 & 2.8 & 3 \\ 0.25 & 0.5 & 0.7 & 1 & 1.2 & 1.5 & 1.7 & 2 & 2.2 & 2.5 & 2.7 & 3 & 3.2 & 3.5 & 3.7 & 4 \\ 0.3 & 0.6 & 0.9 & 1.2 & 1.5 & 1.8 & 2.1 & 2.5 & 2.8 & 3.1 & 3.4 & 3.7 & 4 & 4.3 & 4.6 & 5 \\ 0.37 & 0.7 & 1.1 & 1.5 & 1.8 & 2.2 & 2.6 & 3 & 3.3 & 3.7 & 4.1 & 4.5 & 4.8 & 5.2 & 5.6 & 6 \\ 0.43 & 0.8 & 1.3 & 1.7 & 2.1 & 2.6 & 3 & 3.5 & 3.9 & 4.3 & 4.8 & 5.2 & 5.6 & 6.1 & 6.5 & 7 \\ 0.5 & 1 & 1.5 & 2 & 2.5 & 3 & 3.5 & 4 & 4.5 & 5 & 5.5 & 6 & 6.5 & 7 & 7.5 & 8 \\ 0.56 & 1.1 & 1.6 & 2.2 & 2.8 & 3.3 & 3.9 & 4.5 & 5 & 5.6 & 6.1 & 6.7 & 7.3 & 7.8 & 8.4 & 9 \\ 0.62 & 1.2 & 1.8 & 2.5 & 3.1 & 3.7 & 4.3 & 5 & 5.6 & 6.2 & 6.8 & 7.5 & 8.1 & 8.7 & 9.3 & 10 \\ 0.68 & 1.3 & 2 & 2.7 & 3.4 & 4.1 & 4.8 & 5.5 & 6.1 & 6.8 & 7.5 & 8.2 & 8.9 & 9.6 & 10.3 & 11 \\ 0.7 & 1.5 & 2.2 & 3 & 3.7 & 4.5 & 5.2 & 6 & 6.7 & 7.5 & 8.2 & 9 & 9.7 & 10.5 & 11.2 & 12 \\ 0.8 & 1.6 & 2.4 & 3.2 & 4 & 4.8 & 5.6 & 6.5 & 7.3 & 8.1 & 8.9 & 9.7 & 10.5 & 11.3 & 12.1 & 13 \\ 0.87 & 1.7 & 2.6 & 3.5 & 4.3 & 5.2 & 6.1 & 7 & 7.8 & 8.7 & 9.6 & 10.5 & 11.3 & 12.2 & 13.1 & 14 \\ 0.9 & 1.8 & 2.8 & 3.7 & 4.6 & 5.6 & 6.4 & 7.5 & 8.4 & 9.3 & 10.3 & 11.2 & 12.1 & 13.1 & 14 & 15 \\ 1 & 2 & 3 & 4 & 5 & 6 & 7 & 8 & 9 & 10 & 11 & 12 & 13 & 14 & 15 & 16 \end{bmatrix}.$$

**Example 4.1.1**

In this example two issues are investigated: (1) What happen with coefficients near the boundaries, and (2) What happen with the wavelet coefficients in each one of the three blocks away from the boundaries.

since the original data is not from a periodic function, the periodic extension in boundaries will cause some kind of distortion in both directions.

As we mentioned in two dimensional wavelet decomposition, Figure 10, a function is decomposed into four blocks by transforming it through any wavelet filters, where the low-high subband is related to the horizontal detailed coefficients, and the high-low

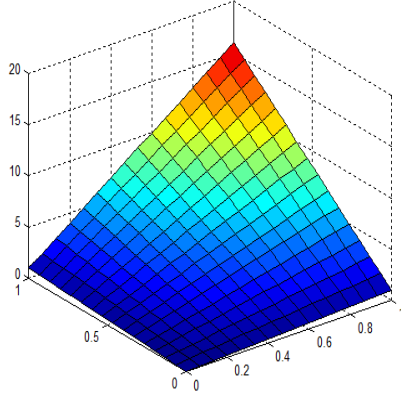


Figure 12: Function  $M = [f_{ij}]_{i,j \in \mathbb{N}}$ , defined  $f_{ij} = i * x_j$  where  $x_j = \frac{j}{16}$  for  $i = 1 : 16$ ,  $j = 1 : 16$ .

subband is mentioned as the vertical detailed coefficients . It means that the low-low block is obtained by moving data through the low pass filter. And the results of the high pass filters yield details, (for data of an image, they represent changes in the location of the image edges).

The *decomposition* of the matrix  $M$  through the two dimension **Db2** wavelet transform is denoted as matrix  $N$  ( $N = 2DWT(M)$ ).

In matrix  $N$ , we can observe the effect in the wavelet transform cause by the property of the vanishing moments. Since Db2 has 2 vanishing moments, the scaling functions represent exactly polynomials with degree 0 and 1. This implies that the wavelet coefficients associated to this transformation for the case of polynomials with degree 0 or 1 must be zero. This is exactly what can be observed inside the domain. All wavelet coefficients are zero inside the domain in all three wavelet blocks. Naturally, because of the effect of the periodization, (the periodic extension of the data) there is a region (exactly in the boundary vicinity) where the wavelet coefficients are no longer zero, because they captured the variation generated by the extension.

$$N = \begin{bmatrix} 0.6 & 1.4 & 2.3 & 3.1 & 3.9 & 4.7 & 5.5 & 5.9 & 0 & 0 & 0 & 0 & 0 & 0 & 0 & 0 & 0 & -1.6 \\ 1.4 & 3.3 & 5.1 & 6.9 & 8.7 & 10.5 & 12.3 & 13.2 & 0 & 0 & 0 & 0 & 0 & 0 & 0 & 0 & 0 & -3.6 \\ 2.3 & 5.1 & 7.9 & 10.7 & 13.5 & 16.3 & 19.2 & 20.5 & 0 & 0 & 0 & 0 & 0 & 0 & 0 & 0 & 0 & -5.6 \\ 3.1 & 6.9 & 10.7 & 14.5 & 18.3 & 22.2 & 26 & 27.7 & 0 & 0 & 0 & 0 & 0 & 0 & 0 & 0 & 0 & -7.6 \\ 3.9 & 8.7 & 13.5 & 18.3 & 23.2 & 28 & 32.8 & 35 & 0 & 0 & 0 & 0 & 0 & 0 & 0 & 0 & 0 & -9.6 \\ 4.7 & 10.5 & 16.3 & 22.2 & 28 & 33.8 & 39.6 & 42 & 0 & 0 & 0 & 0 & 0 & 0 & 0 & 0 & 0 & -1.6 \\ 5.5 & 12.3 & 19.2 & 26 & 32.8 & 39.6 & 46.4 & 49.6 & 0 & 0 & 0 & 0 & 0 & 0 & 0 & 0 & 0 & -133.6 \\ 5.9 & 13.2 & 20.5 & 27.7 & 35 & 42.3 & 49.6 & 53 & 0 & 0 & 0 & 0 & 0 & 0 & 0 & 0 & 0 & -14.5 \\ \hline 0 & 0 & 0 & 0 & 0 & 0 & 0 & 0 & 0 & 0 & 0 & 0 & 0 & 0 & 0 & 0 & 0 & 0 \\ 0 & 0 & 0 & 0 & 0 & 0 & 0 & 0 & 0 & 0 & 0 & 0 & 0 & 0 & 0 & 0 & 0 & 0 \\ 0 & 0 & 0 & 0 & 0 & 0 & 0 & 0 & 0 & 0 & 0 & 0 & 0 & 0 & 0 & 0 & 0 & 0 \\ 0 & 0 & 0 & 0 & 0 & 0 & 0 & 0 & 0 & 0 & 0 & 0 & 0 & 0 & 0 & 0 & 0 & 0 \\ 0 & 0 & 0 & 0 & 0 & 0 & 0 & 0 & 0 & 0 & 0 & 0 & 0 & 0 & 0 & 0 & 0 & 0 \\ 0 & 0 & 0 & 0 & 0 & 0 & 0 & 0 & 0 & 0 & 0 & 0 & 0 & 0 & 0 & 0 & 0 & 0 \\ 0 & 0 & 0 & 0 & 0 & 0 & 0 & 0 & 0 & 0 & 0 & 0 & 0 & 0 & 0 & 0 & 0 & 0 \\ 0 & 0 & 0 & 0 & 0 & 0 & 0 & 0 & 0 & 0 & 0 & 0 & 0 & 0 & 0 & 0 & 0 & 0 \\ -1.6 & -3.6 & -5.6 & -7.6 & -9.6 & -11.6 & -13.6 & -14.5 & 0 & 0 & 0 & 0 & 0 & 0 & 0 & 0 & 0 & 4 \end{bmatrix}.$$

**Example 4.1.2**

In this example we investigate what positions are related in the 4 blocks of wavelet

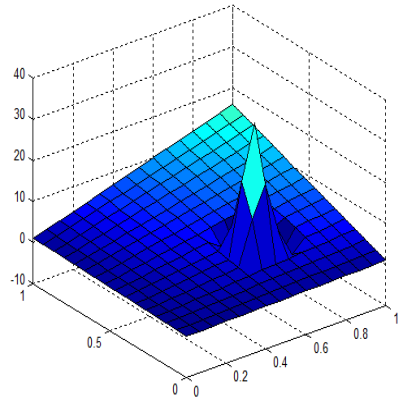
decomposition. That means, if we change just one position of the original matrix, what happen with the wavelet coefficients on the three blocks? Do they change in a specific position? And if one wavelet coefficient is altered, what is the effect of this change in the reconstruction process?

In the above example, we change just the one input value,  $f_{8,8} = 100$  in matrix  $M$  denoted by  $\tilde{M}$ , and apply the bi-dimensional **Db2** wavelet transform ( $\tilde{N} = 2DWT(\tilde{M})$ ). We can notice which values in decomposed matrix  $N$  have changed because of the alteration introduced in the original matrix  $M$ . There are 4 altered values, in each block of the wavelet coefficients effected by this change. Positions of altered values are 2 by 2 blocks start from  $d_{3,3}^V$ ,  $d_{3,3}^H$  and  $d_{3,3}^D$  due to the number of filters in wavelet transform and the decimated algorithm (here cascade algorithm is chose).

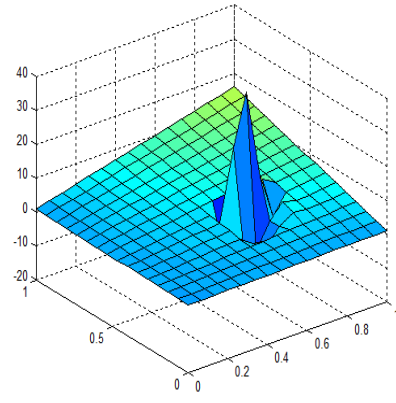
$$\tilde{N} = \begin{bmatrix} 0.6 & 1.4 & 2.3 & 3.1 & 3.9 & 4.7 & 5.5 & 5.9 & 0 & 0 & 0 & 0 & 0 & 0 & 0 & 0 & -1.6 \\ 1.4 & 3.3 & 5.1 & 6.9 & 8.7 & 10.5 & 12.3 & 13.2 & 0 & 0 & 0 & 0 & 0 & 0 & 0 & 0 & -3.6 \\ 2.3 & 5.1 & 11.1 & -10 & 13.5 & 16.3 & 19.2 & 20.5 & 0 & 0 & 0.12 & 5.5 & 0 & 0 & 0 & 0 & -5.6 \\ 3.1 & 6.9 & -10 & 148.9 & 18.3 & 22.2 & 26 & 27.7 & 0 & 0 & -77.5 & -36 & 0 & 0 & 0 & 0 & -7.6 \\ 3.9 & 8.7 & 13.5 & 18.3 & 23.2 & 28 & 32.8 & 35 & 0 & 0 & 0 & 0 & 0 & 0 & 0 & 0 & -9.6 \\ 4.7 & 10.5 & 16.3 & 22.2 & 28 & 33.8 & 39.6 & 42 & 0 & 0 & 0 & 0 & 0 & 0 & 0 & 0 & -1.6 \\ 5.5 & 12.3 & 19.2 & 26 & 32.8 & 39.6 & 46.4 & 49.6 & 0 & 0 & 0 & 0 & 0 & 0 & 0 & 0 & -133.6 \\ 5.9 & 13.2 & 20.5 & 27.7 & 35 & 42.3 & 49.6 & 53 & 0 & 0 & 0 & 0 & 0 & 0 & 0 & 0 & -14.5 \\ \hline 0 & 0 & 0 & 0 & 0 & 0 & 0 & 0 & 0 & 0 & 0 & 0 & 0 & 0 & 0 & 0 & 0 \\ 0 & 0 & 0 & 0 & 0 & 0 & 0 & 0 & 0 & 0 & 0 & 0 & 0 & 0 & 0 & 0 & 0 \\ 0 & 0 & 12 & -77.5 & 0 & 0 & 0 & 0 & 0 & 0 & 44.7 & 20.7 & 0 & 0 & 0 & 0 & 0 \\ 0 & 0 & 5.5 & -36 & 0 & 0 & 0 & 0 & 0 & 0 & 20.7 & 9.6 & 0 & 0 & 0 & 0 & 0 \\ 0 & 0 & 0 & 0 & 0 & 0 & 0 & 0 & 0 & 0 & 0 & 0 & 0 & 0 & 0 & 0 & 0 \\ 0 & 0 & 0 & 0 & 0 & 0 & 0 & 0 & 0 & 0 & 0 & 0 & 0 & 0 & 0 & 0 & 0 \\ 0 & 0 & 0 & 0 & 0 & 0 & 0 & 0 & 0 & 0 & 0 & 0 & 0 & 0 & 0 & 0 & 0 \\ -1.6 & -3.6 & -5.6 & -7.6 & -9.6 & -11.6 & -13.6 & -14.5 & 0 & 0 & 0 & 0 & 0 & 0 & 0 & 0 & 4 \end{bmatrix},$$

In the example 4.1, we change just the one value,  $d_{3,5}^D = 100$ , in decomposed matrix  $N$  and denote the altered matrix by  $N'$ , then we apply the bi-dimensional inverse wavelet transform ( $D^{-1} = 2DIWT(N')$ ) to indicate the effect of this change in reconstruction process. We can notice which values in the reconstruction matrix  $D^{-1}$  have been changed because of the alteration introduced in the diagonal subband of decomposed matrix  $N$ . There are 16 altered values which is a 4 by 4 matrix starts from  $f_{5,9}$ , Figure 13(d). The same changes in position occur due to the changes in the same positions in the scaling, horizontal and vertical blocks, Figure 13.

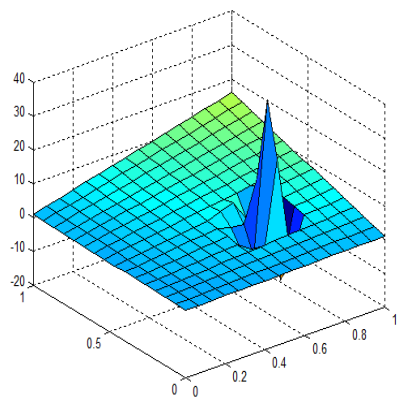
$$D^{-1} = \begin{bmatrix} 0.06 & 0.12 & 0.18 & 0.25 & 0.31 & 0.37 & 0.43 & 0.5 & 0.56 & 0.62 & 0.68 & 0.7 & 0.81 & 0.87 & 0.93 & 1 & \\ 0.12 & 0.25 & 0.37 & 0.5 & 0.62 & 0.7 & 0.87 & 1 & 1.1 & 1.2 & 1.3 & 1.5 & 1.6 & 1.7 & 1.8 & 2 & \\ 0.18 & 0.37 & 0.56 & 0.7 & 0.93 & 1.1 & 1.3 & 1.5 & 1.6 & 1.8 & 2 & 2.2 & 2.4 & 2.6 & 2.8 & 3 & \\ 0.25 & 0.5 & 0.7 & 1 & 1.2 & 1.5 & 1.7 & 2 & 2.2 & 2.5 & 2.7 & 3 & 3.2 & 3.5 & 3.7 & 4 & \\ 0.3 & 0.6 & 0.9 & 1.2 & 1.5 & 1.8 & 2.1 & 2.5 & **3.6** & **4.5** & **-1.9** & **6.8** & 4 & 4.3 & 4.6 & 5 & \\ 0.37 & 0.7 & 1.1 & 1.5 & 1.8 & 2.2 & 2.6 & 3 & **4.8** & **6.2** & **-5.2** & **9.9** & 4.8 & 5.2 & 5.6 & 6 & \\ 0.43 & 0.8 & 1.3 & 1.7 & 2.1 & 2.6 & 3 & 3.5 & **-1.4** & **-5** & **39.8** & **-14.9** & 5.6 & 6.1 & 6.5 & 7 & \\ 0.5 & 1 & 1.5 & 2 & 2.5 & 3 & 3.5 & 4 & **7.6** & **10.4** & **-14.3** & **17.6** & 6.5 & 7 & 7.5 & 8 & \\ 0.56 & 1.1 & 1.6 & 2.2 & 2.8 & 3.3 & 3.9 & 4.5 & 5 & 5.6 & 6.1 & 6.7 & 7.3 & 7.8 & 8.4 & 9 & \\ 0.62 & 1.2 & 1.8 & 2.5 & 3.1 & 3.7 & 4.3 & 5 & 5.6 & 6.2 & 6.8 & 7.5 & 8.1 & 8.7 & 9.3 & 10 & \\ 0.68 & 1.3 & 2 & 2.7 & 3.4 & 4.1 & 4.8 & 5.5 & 6.1 & 6.8 & 7.5 & 8.2 & 8.9 & 9.6 & 10.3 & 11 & \\ 0.7 & 1.5 & 2.2 & 3 & 3.7 & 4.5 & 5.2 & 6 & 6.7 & 7.5 & 8.2 & 9 & 9.7 & 10.5 & 11.2 & 12 & \\ 0.8 & 1.6 & 2.4 & 3.2 & 4 & 4.8 & 5.6 & 6.5 & 7.3 & 8.1 & 8.9 & 9.7 & 10.5 & 11.3 & 12.1 & 13 & \\ 0.87 & 1.7 & 2.6 & 3.5 & 4.3 & 5.2 & 6.1 & 7 & 7.8 & 8.7 & 9.6 & 10.5 & 11.3 & 12.2 & 13.1 & 14 & \\ 0.9 & 1.8 & 2.8 & 3.7 & 4.6 & 5.6 & 6.5 & 7.5 & 8.4 & 9.3 & 10.3 & 11.2 & 12.1 & 13.1 & 14 & 15 & \\ 1 & 2 & 3 & 4 & 5 & 6 & 7 & 8 & 9 & 10 & 11 & 12 & 13 & 14 & 15 & 16 & \end{bmatrix}.$$



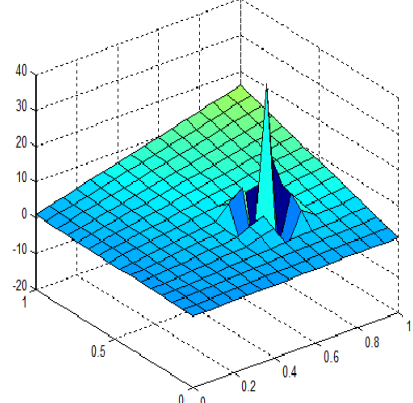
(a)



(b)



(c)



(d)

Figure 13: (a) Shows the reconstruction of the matrix  $N$  with change in the scaling block i.e  $f_{3,5} = 100$ . (b) Depicts the reconstruction of the matrix  $N$  with change in position  $(3,5)$  in horizontal block ( $f_{11,5} = 100$ ). (c) Shows the inverse of the matrix  $N$  with change in position  $(3,5)$  in vertical block ( $f_{3,13}$ ). (d) Illustrates the inverse of the matrix  $N$  with changes in the position  $(3,5)$  in diagonal block, ( $D^{-1}$ ).

## 5 Microcalcifications detection in Mammography

In the last 2 decades, several mammography processing methods have been developed to detect microcalcifications by radiologist where among them wavelets transforms have been exploited efficiently. In this section we apply 2D wavelet transform as described in section 4 on mammographies in order to analyze and to identify strong variations contained within the mammogram images.

The mammogram images presented here, scanned as raw format with 8-bit grayscale and 256 by 256 pixel size, were obtained from the University of South Florida Digital Mammography Home page [18].

The main goal of this section is to detect the microcalcifications in mammographies by exploring concepts of wavelets transforms and statistical measurements such as skewness and kurtosis parameters. In this case mammogram images are decomposed by Db2 wavelet transform into four different subbands (1 level decimated decompositions).

Here we consider two different mammographies of the mentioned website. Figure 14a is the right breast mammogram image suspected as a mammogram with some microcalcifications clusters, and Figure 14b is the left breast mammogram image with normal tissues such as blood vessels and mammary ducts.

According to [11], in microcalcifications regions the symmetry of the Gaussian distribution of wavelet coefficients is destroyed and the tails of their distribution are heavier. The statistical quantities able to identify these deformations in the shape of the Gaussian distributions are the third and fourth order correlation parameters, called skewness and kurtosis, respectively.

So in order to have the exact detection we calculate the quantities of skewness and kurtosis of wavelet coefficients and threshold wavelet coefficients for row and column directions separately. After thresholding, the positions (intersections of rows and columns) associated to the significant values are identified. The regions of interest (areas of microcalcifications in mammography) are obtained as intersection of the significant rows and columns. Remembering that significant values are those greater than the threshold values.

### 5.1 Wavelets Representation of Images

In the Section 4, we indicated how an image matrix  $M$  is decomposed into four different subbands through the wavelet filters in 1 level decomposition (see Figure 10).

The subband  $H_y H_x M$  (called C) contains the smooth information of the image (background), and the subbands  $H_y G_x M, G_y H_x M$  and  $G_y G_x M$  (called V, H, D, respectively) contain the detail information of the image (edges).

The properties of wavelet transform show that the significant information of an image can be extracted by eliminating the subband of the wavelet decomposed image that contains the lowest frequencies (subband C) [15]. Reconstructing the wavelet components individually (subbands V, H, D) gives us the vertical, horizontal and diagonal edges.

In other words, each pixel in an image has two pixels in the horizontal, two in the vertical and four in the diagonal directions in its neighborhood. For instance, vertical

edge points of an image occur, if the variation of the pixel value (in the specific location) is small in the vertical direction. So all eight different pixels in variations are calculated by considering the wavelet coefficients in decomposed image before reconstruction.

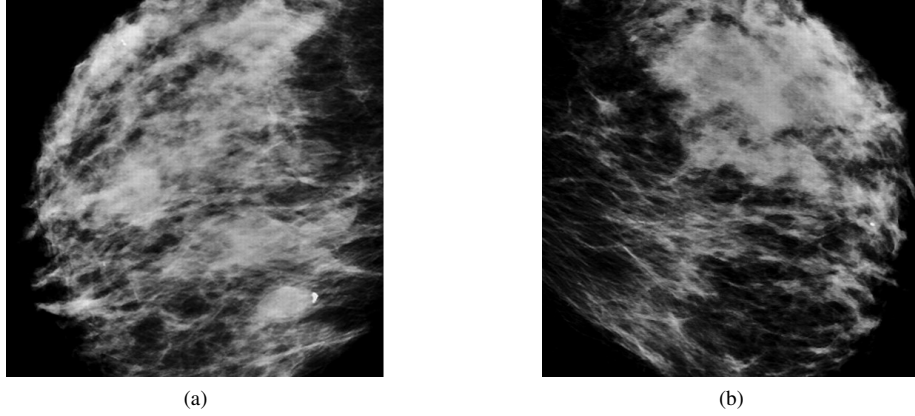


Figure 14: (a) Right breast mammography with microcalcifications. (b) left breast mammography with normal tissues.

## 5.2 Thresholding

### 5.2.1 Soft Thresholding

The wavelet coefficients  $d_{j,k}^i$  where  $i$  indicates vertical, horizontal and diagonal subbands are obtained by applying the specific wavelets transform on an image. The soft thresholding method on the wavelet coefficients  $d_{j,k}^i$  can be performed as:

$$s_{j,k}^i = \begin{cases} d_{j,k}^i - \lambda^i & \text{if } d_{j,k}^i > \lambda^i \\ d_{j,k}^i + \lambda^i & \text{if } d_{j,k}^i < -\lambda^i \\ 0 & \text{otherwise,} \end{cases} \quad (5.1)$$

where  $s_{j,k}^i$  are the threshold wavelet coefficients, and  $\lambda^i$  is the threshold value.

Now we modify the soft thresholding formula and amplify the wavelet coefficients by:

$$s'_{j,k}{}^i = \begin{cases} d_{j,k}^i + \lambda^i & \text{if } d_{j,k}^i > \lambda^i \\ d_{j,k}^i - \lambda^i & \text{if } d_{j,k}^i < -\lambda^i \\ 0 & \text{otherwise,} \end{cases} \quad (5.2)$$

where  $s'_{j,k}{}^i$  are the threshold wavelet coefficients.

### 5.2.2 Hard thresholding

Hard thresholding is another filtering method that is applied on the wavelet coefficients in the following way:

$$s_{j,k}^i = \begin{cases} d_{j,k}^i & \text{if } |d_{j,k}^i| \geq \lambda^i \\ 0 & \text{if } |d_{j,k}^i| < \lambda^i, \end{cases} \quad (5.3)$$

where  $\lambda^i$  is threshold value for subband  $i$ . In this process, wavelet coefficients are suppressed if the values are less than the threshold, and they are kept if they are greater than the threshold.

There are several methods to calculate the threshold value  $\lambda^i$ , here we use a statistical method to calculate this value. In this case  $\lambda^i$  is calculated from

$$\lambda^i = \mu^i + \alpha \sigma^i, \quad (5.4)$$

where  $\mu^i$  is the mean value of the wavelet coefficients for subband  $i$ ,  $\sigma^i$  is the standard deviation of the wavelet coefficients for subband  $i$ .

---

#### Algorithm 4 Edge Detection

---

Input: image (I)

1) WT (I)=(C, V, H, D), 1 level Db2 wavelet transform

2)  $\tilde{V} = Thr(\tilde{V})$ ,  $\tilde{H} = Thr(\tilde{H})$ ,  $\tilde{D} = Thr(\tilde{D})$ , Soft and hard thresholding

3)  $\widetilde{I_{Edge}} = IWT(0, \tilde{V}, \tilde{H}, \tilde{D})$ , Inverse wavelet transform of threshold detail coefficients

Output: image ( $\widetilde{I_{Edge}}$ ) with changes in the scale, new pixels=1-old pixels

---

#### Example 5.1.

Consider a mammography with several clusters formed by microcalcifications (Figure 14a). In order to detect these abnormal textures the algorithm 4 is performed on this image.

Figure 15 shows the output images with 3 different threshold methods on wavelet coefficients. The inverse wavelet transform of soft threshold wavelet coefficients (Figure 15a), modified soft threshold wavelet coefficients (Figure 15b) and hard threshold wavelet coefficients (Figure 15c) are depicted, respectively.

Using the modified soft threshold method amplifies the wavelet coefficients and provides enhancements in the microcalcifications regions.

From what is clarified in Figure 15, Db2 wavelet transform detects big numbers of pixels where some of them belong to microcalcifications. Thus shorter wavelet filters are more sensitive to extract microcalcifications, however, they tend to produce more false positive numbers.

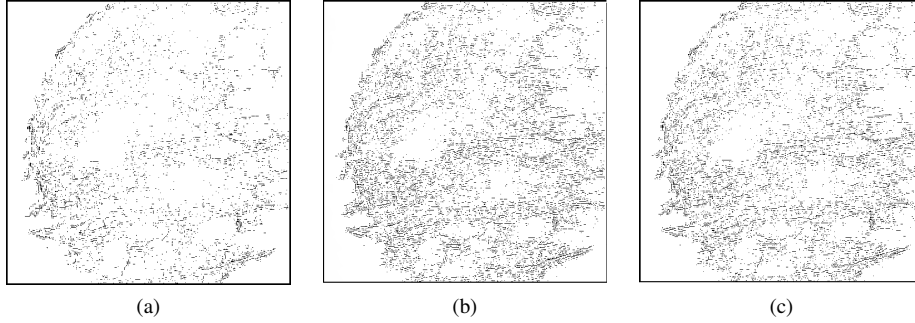


Figure 15: (a) Edge detection using the soft thresholding method. (b) Edge detection using the modified soft thresholding method. (c) Edge detection using the hard thresholding method.

### 5.3 Detection Parameters: Skewness and Kurtosis

In the previous subsection we observed that some of the pixels detected after thresholding the wavelet coefficients are microcalcifications. So in order to have exact detection rates (to classify information associated to microcalcifications) statistical measures (skewness and kurtosis parameters) have been applied to the wavelet coefficients of the transformed mammographies [11, 14].

**Definition 5.1.** For a sample of  $n$  values, skewness (S) parameter is defined as:

$$S = \frac{\frac{1}{n} \sum_{l=1}^n (x_l - \bar{x})^3}{\left(\frac{1}{n} \sum_{l=1}^n (x_l - \bar{x})^2\right)^{3/2}}, \quad (5.5)$$

where  $\bar{x}$  is the sample mean.

Skewness is a measure of the degree of asymmetry of a distribution. The skewness value can be positive or negative, or even undefined [17].

A negative skewness indicates that the tail on the left side of the probability density function is longer than the right side and the bulk of the values (possibly including the median) lie to the right of the mean. A positive skewness indicates that the tail on the right side is longer than the left side and the bulk of the values lie to the left of the mean, see Figure 16.

An understanding of the skewness of the data set indicates whether deviations from the mean are going to be positive or negative, So the normal distribution (data are symmetric about the mean) has a skewness of zero.

**Definition 5.2.** For a sample of  $n$  values, kurtosis (K) parameters is defined as:

$$K = \frac{\frac{1}{n} \sum_{l=1}^n (x_l - \bar{x})^4}{\left(\frac{1}{n} \sum_{l=1}^n (x_l - \bar{x})^2\right)^2} - 3, \quad (5.6)$$

where  $\bar{x}$  is the sample mean.

Kurtosis is the degree of peakedness of a distribution [17]. A distribution with positive

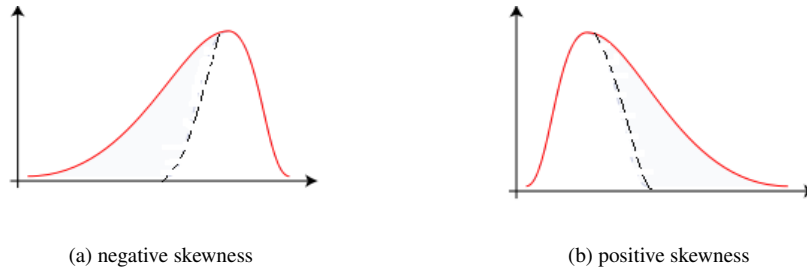


Figure 16: (a) The left tail is longer and the mass of the distribution is concentrated on the right of the figure. (b) The right tail is longer and the mass of the distribution is concentrated on the left of the figure.

kurtosis has a sharper peak and longer tails, while a distribution with negative kurtosis has a more rounded peak and shorter tails, Figure 17. Normal distribution is the most prominent example of distribution with zero kurtosis.

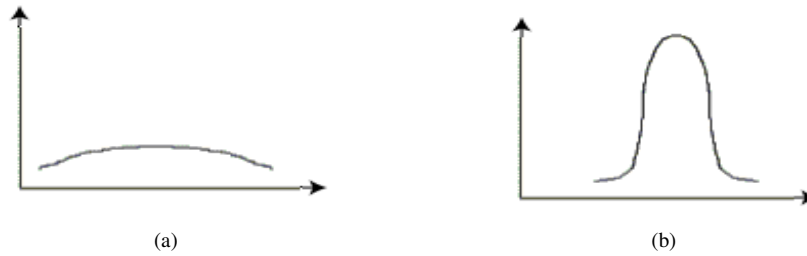


Figure 17: (a) Negative kurtosis. (b) Positive kurtosis.

### 5.3.1 Numerical Experiments

According to [11], if a region contains microcalcifications then the symmetry of the distribution of wavelet coefficients is destroyed. Figure 18 and 19 show histograms of wavelet coefficients of Figure 14a and 14b, respectively. The skewness and kurtosis values clarified here for abnormal tests are greater than those for normal ones.

#### 5.3.1.1 Numerical Experiments of Skewness

In this subsection, we compute the skewness of mammographies before and after wavelet thresholding, since we want to investigate if a previous thresholding stage of the wavelet coefficients can help in the microcalcifications detection.

Algorithm 5 and 6 indicate the process to point out the regions of interest in mammographies by calculating skewness values of wavelet coefficients and threshold wavelet coefficients, respectively.

### Wavelet Coefficients Histogram of the Mammography with Microcalcifications

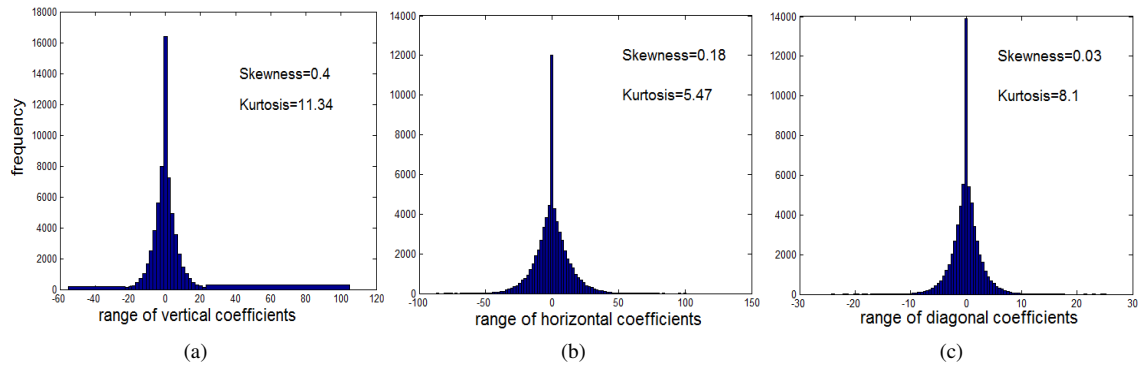


Figure 18: (a) Vertical coefficients histogram . (b) Horizontal coefficients histogram. (c) Diagonal coefficients histogram

### Wavelet Coefficients Histogram of the Mammography without microcalcifications

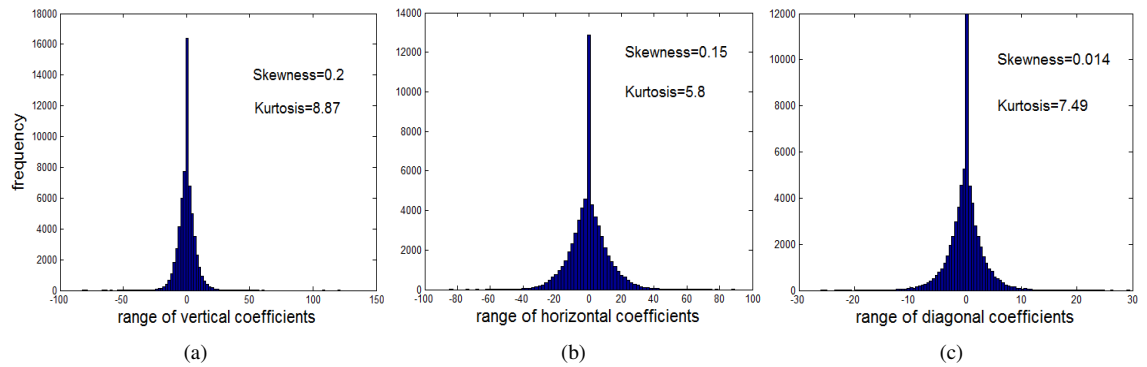


Figure 19: (a) Vertical coefficients histogram . (b) Horizontal coefficients histogram. (c) Diagonal coefficients histogram

#### Example 5.2.

In this example we apply the algorithm 5 on two main blocks of simulations considering input data images with and without microcalcifications, Figure 14a and 14b.

From what is clarified in Figure 18, the distributions of wavelet coefficients for each subband are not normal and has skewness.

The row and column skewness values for each mentioned mammography are depicted in Figure 20 and 21, respectively. The horizontal lines in each subplot point the threshold values of each row and column subbands skewness.

After thresholding the skewness values, the sample 108 of row skewness and sample 120 of column skewness have the high skewness values for all wavelet coefficients,

Figure 20, where the intersection of them (point (219, 243) in Figure 14a) detects one of the most important calcifications, Figure 28. While the threshold skewness values for mammography without calcifications in Figure 21 do not indicate the common significant rows and columns, and the skewness values approach to the normal distribution, since the distributions of wavelet coefficients for each subband tend to normal.

---

**Algorithm 5** Skewness Calculation via Wavelet Coefficients

---

Input: image (I)

- 1) WT (I)=(C, V, H, D), 1 level Db2 wavelet transform
- 2)  $S^r(V), S^r(H), S^r(D)$ , skewness computed for each line of the subbands V, H, D
- 3)  $S^c(V), S^c(H), S^c(D)$ , skewness computed for each column of the subbands V, H, D
- 4) Threshold of  $S^r(\cdot), S^c(\cdot)$
- 4.1) Compute max skewness value of each subband
- 4.2)  $T = 0.75 * \max|S_i|$ , where  $i=V, H, D$  threshold value of each subband
- 4.3)  $\tilde{S}_i$ = hard threshold  $S_i$
- 5) The significant rows and columns are obtained after thresholding.

Output: Regions are selected as being neighborhoods of the crossing of significant rows and columns.

---



---

**Algorithm 6** Skewness Calculation via Threshold Wavelet Coefficients

---

Input: image (I)

- 1) WT (I)=(C, V, H, D), 1 level Db2 wavelet transform
- 2)  $\tilde{V} = Thr(\tilde{V}), \tilde{H} = Thr(\tilde{H}), \tilde{D} = Thr(\tilde{D})$ , hard thresholding of wavelet coefficients
- 3)  $S^r(\tilde{V}), S^r(\tilde{H}), S^r(\tilde{D})$ , skewness computed for each line of the subbands V, H, D
- 4)  $S^c(\tilde{V}), S^c(\tilde{H}), S^c(\tilde{D})$ , skewness computed for each column of the subbands V, H, D
- 5) The significant rows and columns are obtained.

Output: Regions are selected as being neighborhoods of the crossing of significant rows and columns.

---

**Example 5.3.**

In this example, algorithm 6 is applied on the aforesaid images in example 5.2.

Figure 22 and 23 show the skewness values of threshold wavelet coefficients. For the mammographies with calcifications the same sample as nonthreshold wavelet coefficients has the high row and column skewness. And it is marked as the region of interest, Figure 28.

**5.3.1.2 Numerical Experiment of Kurtosis**

In this subsection, we compute another statistical parameter based on kurtosis. The high kurtosis values of wavelet coefficients can determine the regions of interest in mammography.

Performing algorithms 7 and 8 on mammographies leads to investigate regions of microcalcifications.

Following two examples indicate how these algorithms process to mark the significant rows and columns.

### Subbands Skewness Case with Calcifications

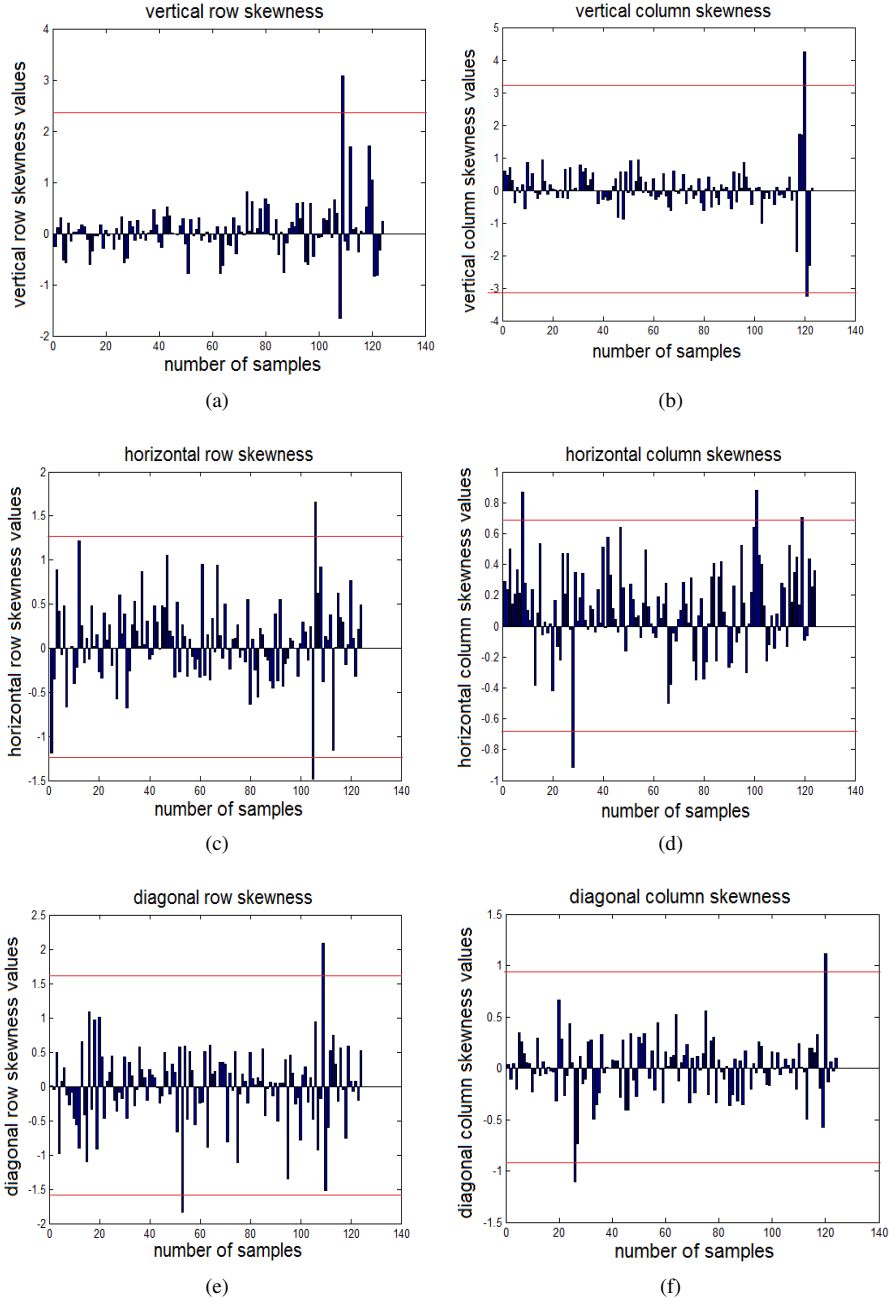


Figure 20: (a) Row skewness values of vertical subband of malignant mammography. (b) Column skewness values of vertical subband of malignant mammography. (c) Row skewness values of horizontal subband of malignant mammography. (d) Column skewness values of horizontal subband of malignant mammography. (e) Row skewness values of diagonal subband of malignant mammography. (f) Column skewness values of diagonal subband of malignant mammography.

### Subbands Skewness Case without Calcifications

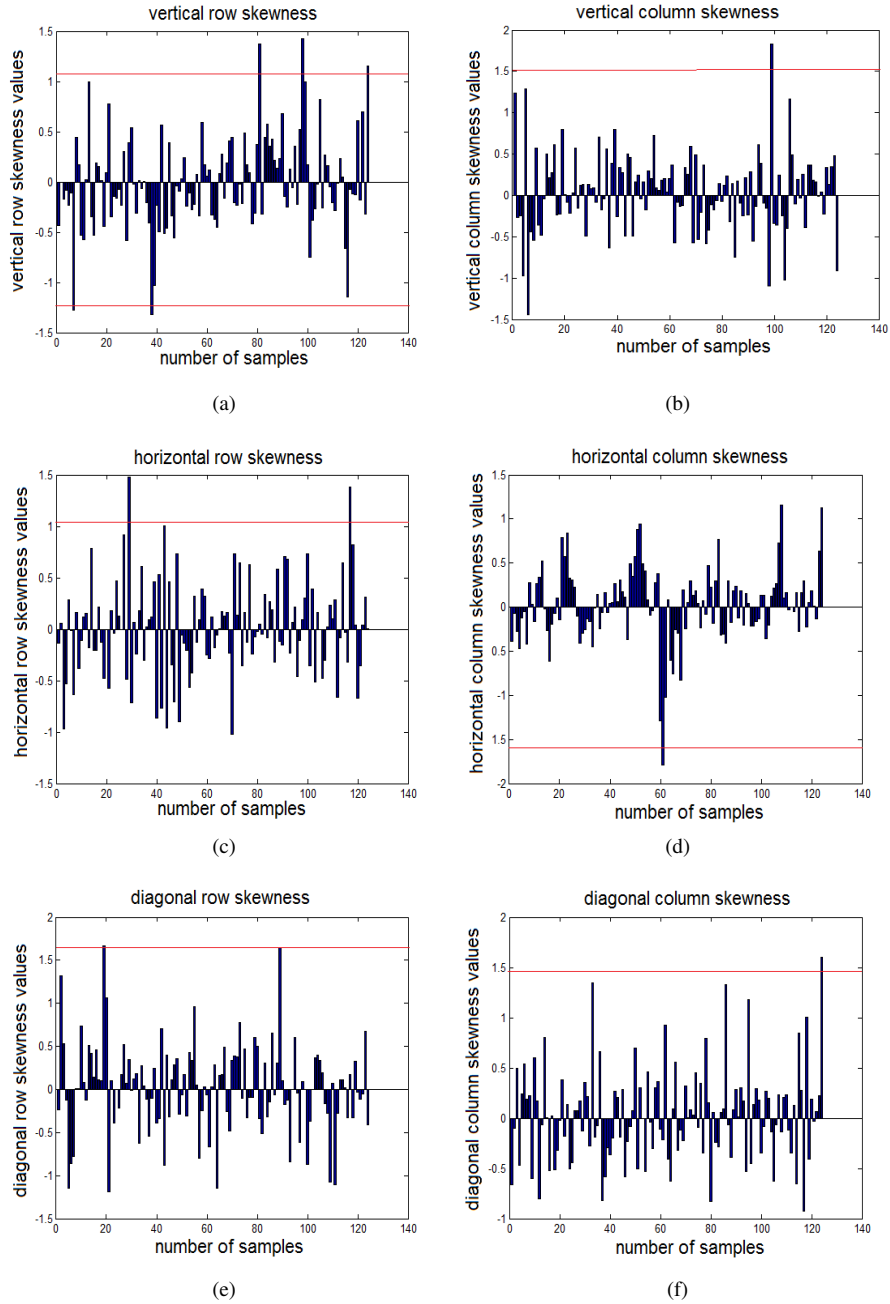


Figure 21: (a) Row skewness values of vertical subband of normal mammography. (b) Column skewness values of vertical subband of normal mammography. (c) Row skewness values of horizontal subband of normal mammography. (d) Column skewness values of horizontal subband of normal mammography. (e) Row skewness values of diagonal subband of normal mammography. (f) Column skewness values of diagonal subband of normal mammography.

### Threshold Subbands Skewness Case with Calcifications

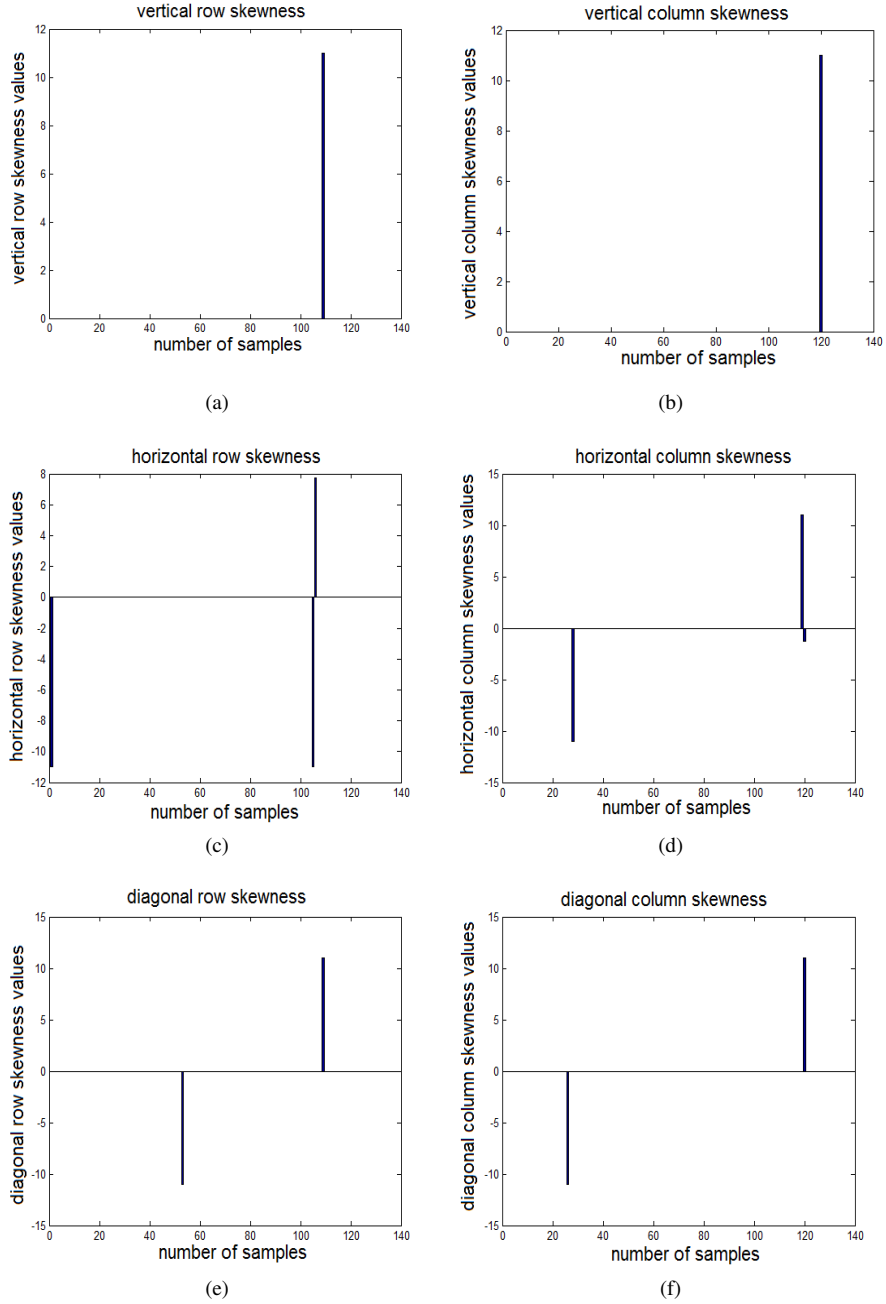


Figure 22: (a), (c), (e) Row skewness values of threshold subbands of malignant mammography. (d), (e), (f) Column skewness values of threshold subbands of malignant mammography.

### Threshold Subbands Skewness Case without Calcifications

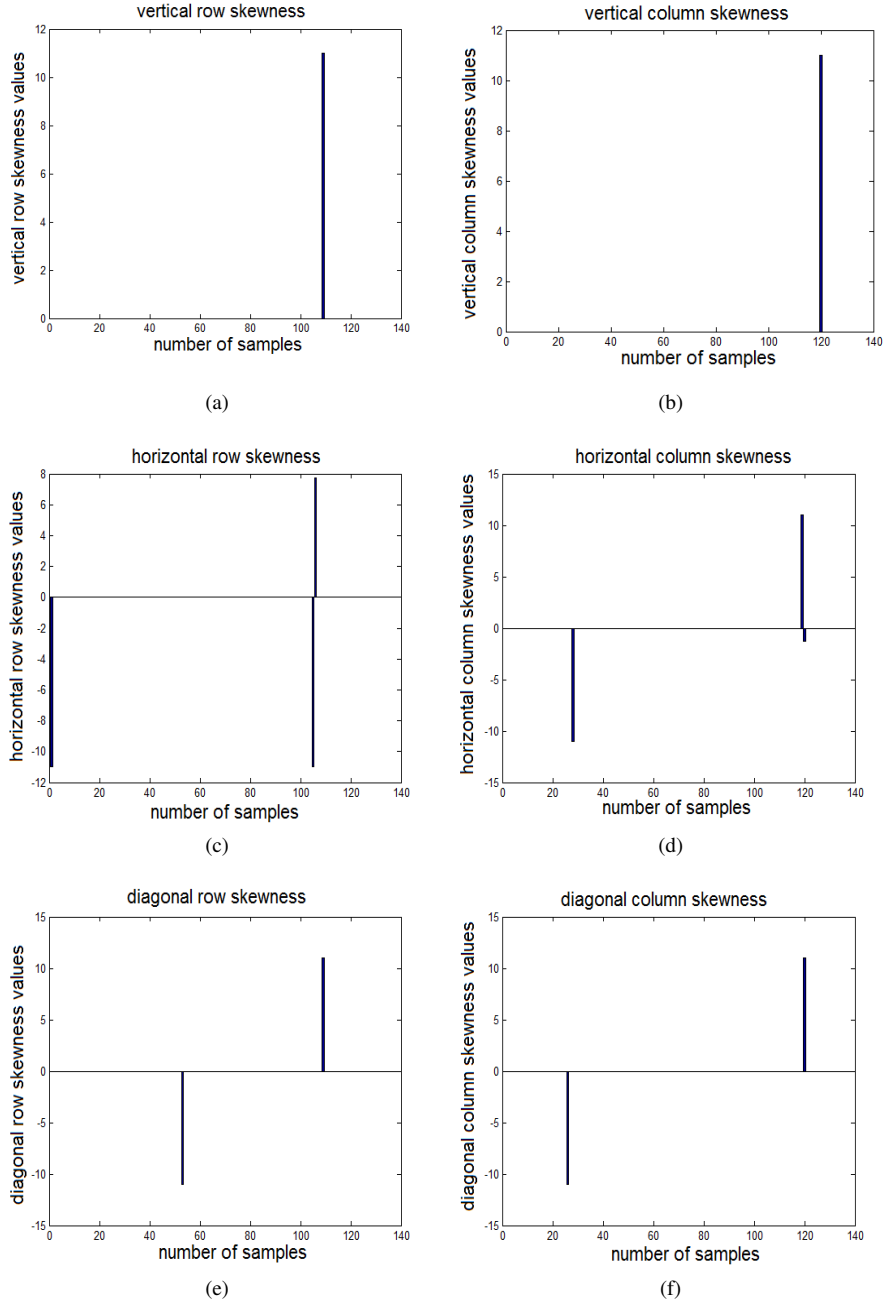


Figure 23: (a), (c), (e) Row skewness values of threshold subbands of normal mammography. (b), (d), (f) Column skewness values of threshold subbands of normal mammography.

---

**Algorithm 7** Kurtosis Calculation via Wavelet Coefficients

---

Input: image (I)

- 1) WT (I)=(C,V,H,D), 1 level Db2 wavelet transform
- 2)  $K^r(V), K^r(H), K^r(D)$ , kurtosis computed for each line of the subbands V, H, D
- 3)  $K^c(V), K^c(H), K^c(D)$ , kurtosis computed for each column of the subbands V, H, D
- 4) Threshold of  $K^r(\cdot), K^c(\cdot)$ 
  - 4.1) Compute max kurtosis value of each subband
  - 4.2)  $T = 0.75 * \max|K_i|$ , where  $i=V, H, D$  threshold value of each subband
  - 4.3)  $\tilde{K}_i$ = hard threshold  $K_i$
- 5) The significant rows and significant columns are obtained after thresholding.

Output: Regions are selected as being neighborhoods of the crossing of significant rows and columns.

---

---

**Algorithm 8** Kurtosis Calculation via Threshold Wavelet Coefficients

---

Input: image (I)

- 1) WT (I)=(C,V,H,D), 1 level Db2 wavelet transform
- 2)  $\tilde{V} = Thr(\tilde{V}), \tilde{H} = Thr(\tilde{H}), \tilde{D} = Thr(\tilde{D})$ , hard thresholding of wavelet coefficients
- 3)  $K^r(\tilde{V}), K^r(\tilde{H}), K^r(\tilde{D})$ , kurtosis computed for each line of the subbands V, H, D
- 4)  $K^c(\tilde{V}), K^c(\tilde{H}), K^c(\tilde{D})$ , kurtosis computed for each column of the subbands V, H, D
- 5) The significant rows and significant columns are obtained .

Output: Regions are selected as being neighborhoods of the crossing of significant rows and columns.

---

**Example 5.4.**

In this example we apply the algorithm 7 on two main block of simulations considering input data images with and without microcalcifications, see Figure 14a and 14b.

The row and column kurtosis values for each mentioned mammography are depicted in Figure 24 and 25, respectively. The horizontal lines in each subplot point the threshold values of each row and column wavelet subbands kurtosis.

From what is clarified in Figure 24, after thresholding the kurtosis values, the sample 108 of row kurtosis and sample 120 of column kurtosis have the highest kurtosis values for all wavelet coefficients (same as in the case of skewness computation in example 5.2), where the intersection of them (point (219,243) in Figure 14a) indicates one of the most important calcifications, Figure 28. Whereas the threshold kurtosis values for mammography without calcifications in Figure 25 do not indicate the common significant rows and columns, and the kurtosis values approach to the normal distribution.

**Example 5.5.**

In this example, the algorithm 8 is applied on the aforesaid mammographies in example 5.4.

Figure 26 and 27 show the kurtosis of threshold wavelet coefficients. For the mammography with calcifications the same samples as nonthreshold wavelet coefficients have high row and column kurtosis.

### Subbands Kurtosis Case with Calcifications

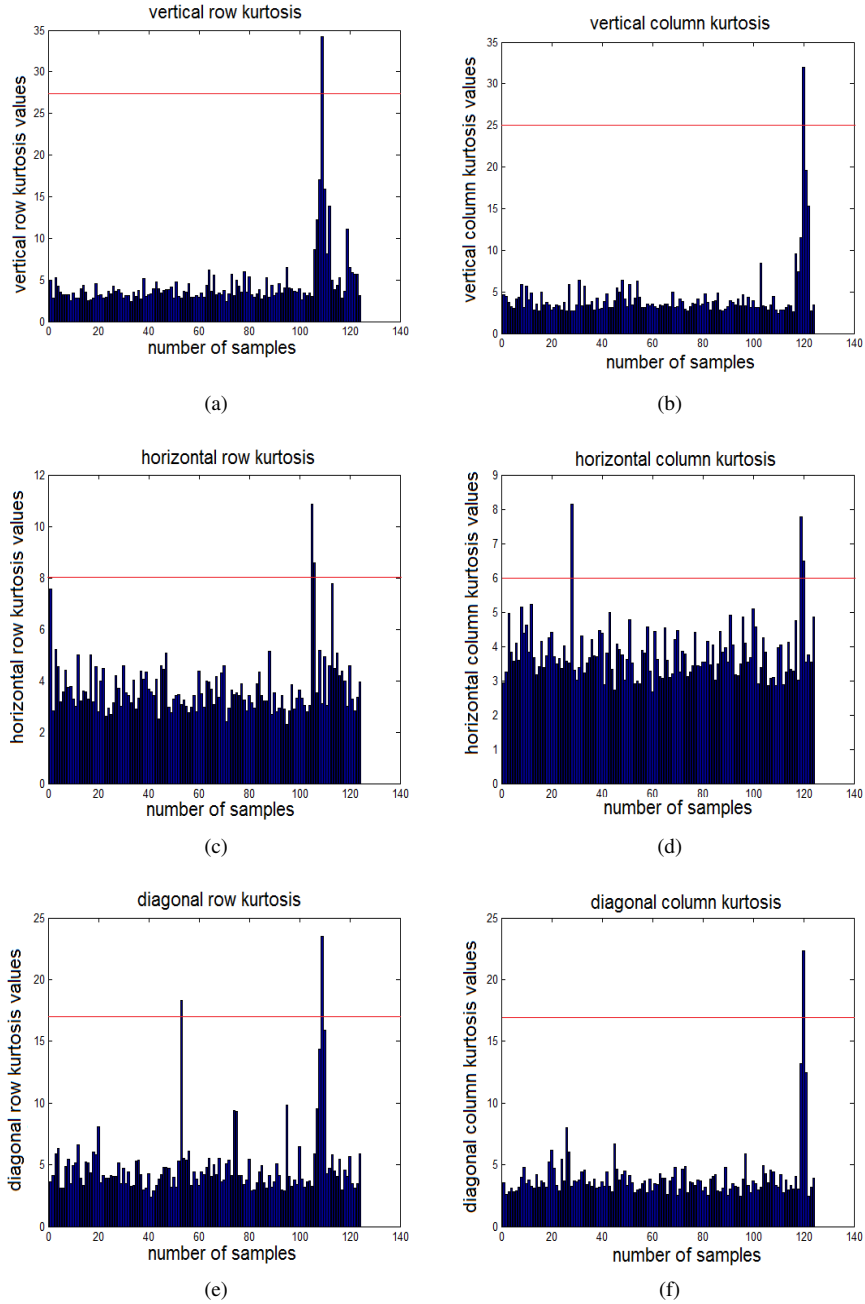


Figure 24: (a), (c), (e) Row wavelet subbands kurtosis of malignant mammography. (b), (d), (f) Column wavelet subbands kurtosis of malignant mammography.

### Subbands Kurtosis Case without Calcifications

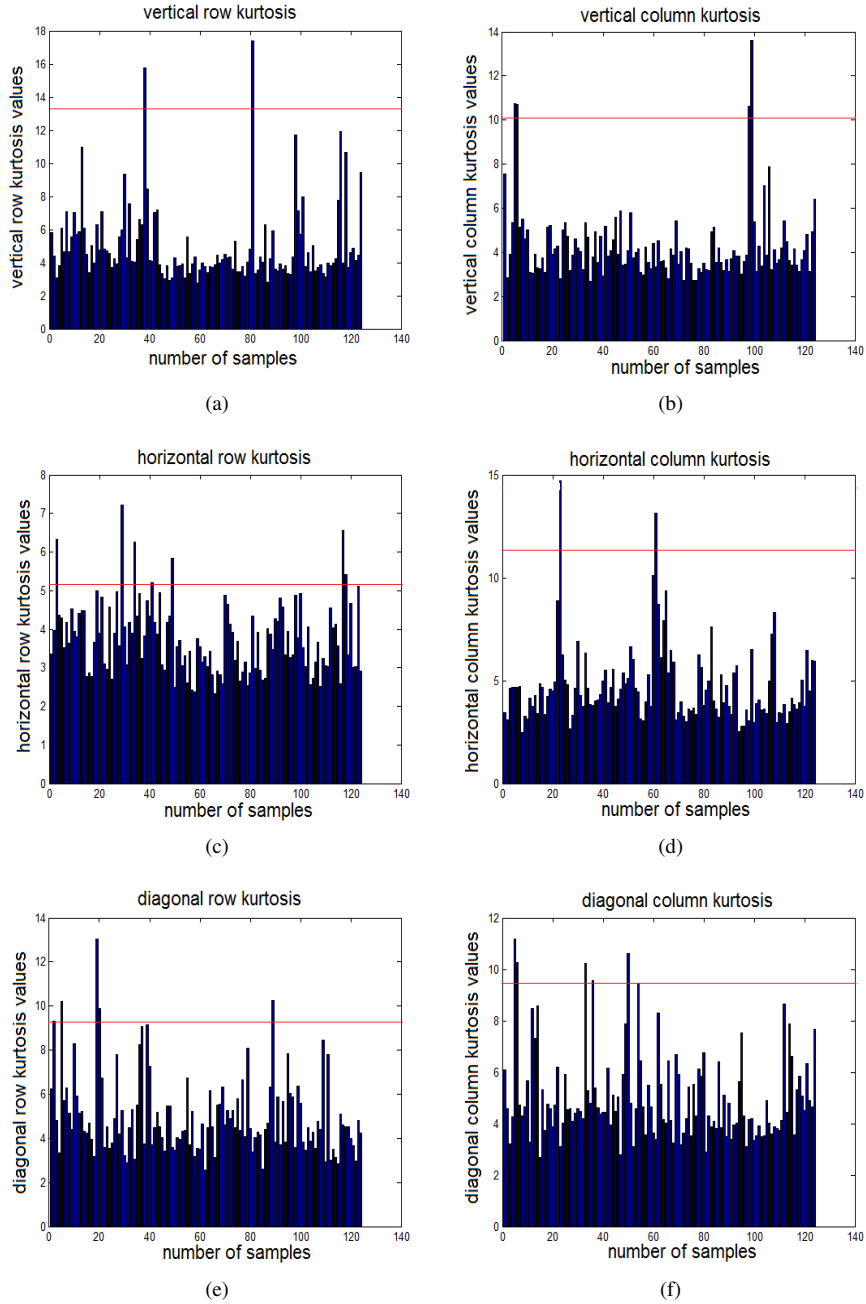


Figure 25: (a), (c), (e) Row wavelet subbands kurtosis of normal mammography. (b), (d), (f) Column wavelet subbands kurtosis of normal mammography.

### Threshold Subbands Kurtosis Case with Calcifications

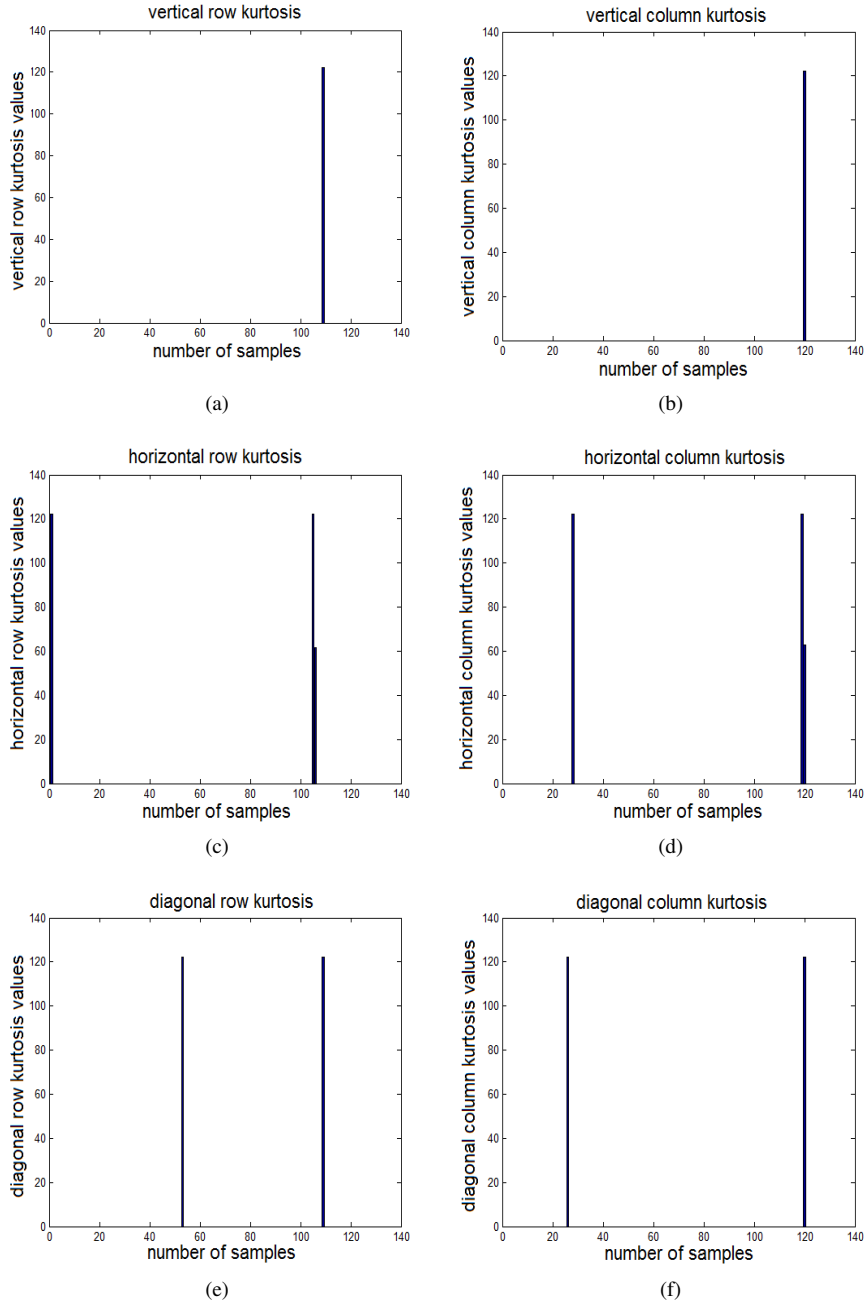


Figure 26: (a), (b), (c) Row kurtosis values of threshold vertical, horizontal and diagonal subbands of malignant mammography. (d), (e), (f) Column kurtosis values of threshold vertical, horizontal and diagonal subbands of malignant mammography.

### Threshold Subbands Kurtosis Case without Calcifications

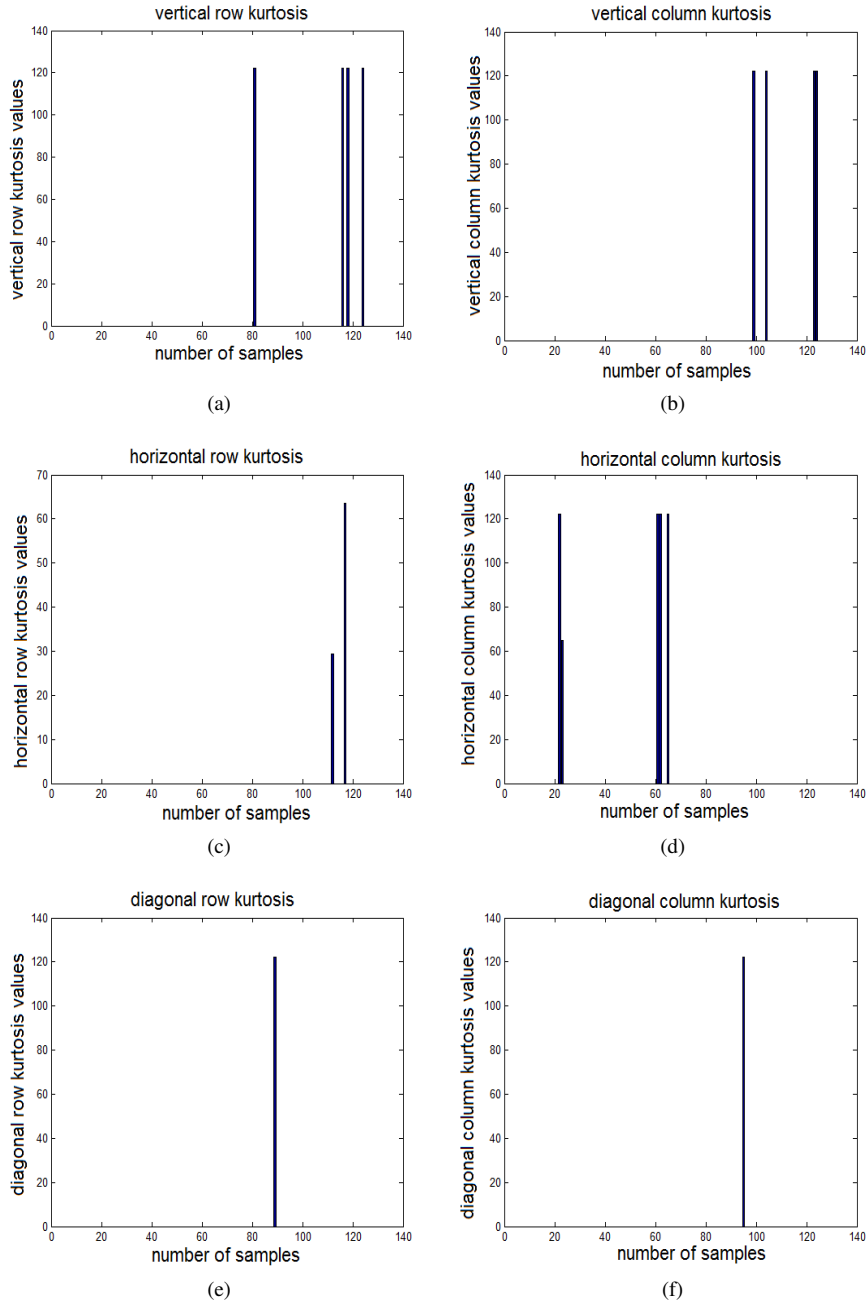


Figure 27: (a), (b), (c) Row kurtosis values of threshold vertical, horizontal and diagonal subbands of normal mammography. (d), (e), (f) Column kurtosis values of threshold vertical, horizontal and diagonal subbands of normal mammography.

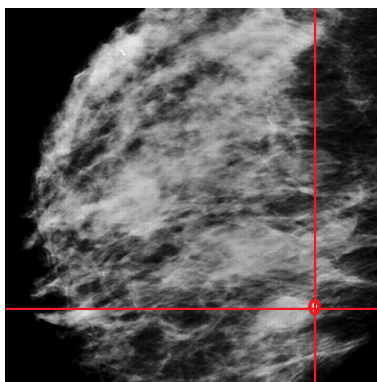


Figure 28: The region of interest selected as being neighborhood of the crossing of significant row and column.

## 5.4 Result and Discussion

In subsection 5.3, microcalcifications regions in mammographies have been detected by performing algorithms using wavelet transforms and statistical measurements. We calculated the quantities of skewness and kurtosis of wavelet coefficients for both (rows and columns) directions, separately. The intersections of rows and columns associated to the significant values are marked as areas of microcalcifications, see Figure 29b.

Now we apply the aforesaid algorithms without performing any wavelet transforms in order to investigate if a previous filtering stage of an image is necessary to detect microcalcifications. It means that, the values of skewness and kurtosis of mammogram images for row and column directions are calculated directly for the image data. The intersections of rows and columns associated to the significant values for skewness and kurtosis are again marked. Nevertheless for this experiment some false positives results were obtained. Blocks in mammographies were assigned to calcification clusters, where in fact no malignant tissue was present, see Figure 29c.

This experiment indicates the relevance of the wavelet coefficients for the correct analysis.

Another preliminary experiments presented in subsection 5.3 indicates that remarkably similar outcomes for calcification clusters detection were obtained when thresholded and non thresholded wavelet coefficients were considered for the computation of skewness and kurtosis.

In order to evaluate the results of the proposed detection methods, we perform a statistical test based on skewness and kurtosis on 24 digitized mammographies obtained as scanned raw format with 8-bit grayscale and 256 by 256 pixel size where 18 of them are suspected as mammographies with microcalcifications.

According to [11], the microcalcifications detection method is posed as a hypothesis testing problem in which the null hypothesis,  $H_0$ , corresponds to the case of no microcalcifications against the alternative  $H_1$ , and it follows the rule  $\Gamma$  based on skewness

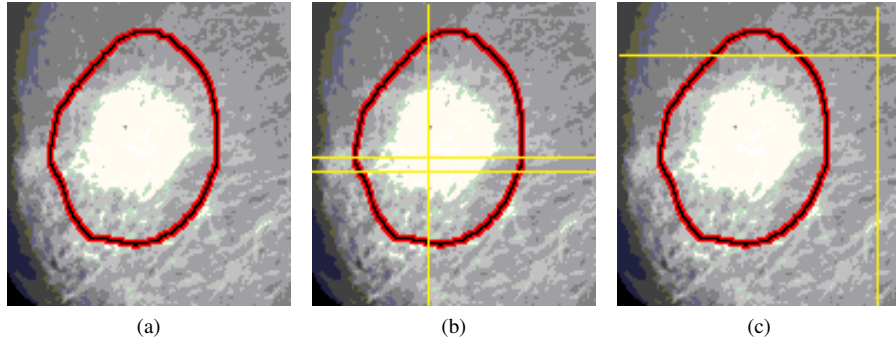


Figure 29: (a) Mammography with malignant tissue marked with physicians. (b) Two regions of interest selected as being neighborhood of the crossing of significant row and columns obtained by calculating skewness and kurtosis values of wavelet coefficients. (c) A region selected as being neighborhood of the crossing of significant row and columns obtained by the analysis of skewness and kurtosis computed directly from the image data, where indicates no interested tissues.

and kurtosis values,

$$\Gamma(x) = \begin{cases} 0 & S_i < T_i \text{ or } K_i < T_i \\ 1 & S_i \geq T_i \text{ and } K_i \geq T_i, \end{cases} \quad (5.7)$$

where  $T_i$  is the threshold values determined slightly below the maxima of the row and column skewness and kurtosis values of each subband.

Table 1 shows the proceeds of the aforesaid statistical test on the mentioned mammographies. For the normal mammographies, no regions of interest are detected by this test, which characterizes 100% of correct detection.

For the cases where the mammographies presented abnormal formations, the detection algorithm also performed properly. Nevertheless in some cases, some malignant regions were over detected, with several crossings inside the same region, as presented in Figure 29b.

The red curves in Figure 29 are the indicated areas containing malignant clusters, according to [18].

## 6 Conclusion

This thesis concerns an approach to detect microcalcifications of mammographies based on the wavelets transforms.

In fact, the potential of wavelet-based subbands of image decompositions are exploited to extract the microcalcifications.

Using decimated Db2 wavelet transform, and reconstructing first level threshold wavelet coefficients we have been able to detect the edges of image, where in the case of mammographies, some of the detections are microcalcifications and the others are false numbers.

In order to have more reliable detection, statistical methods based on the skewness and kurtosis concepts are proposed. These parameters are the measures of the asymmetry of the subbands distributions, where high values represents the microcalcifications.

Based on the numerical results, we come up to the conclusion that the high skewness and kurtosis values of wavelet coefficients and threshold wavelet coefficients indicate same regions.

Hence the previous thresholding stage of the wavelet coefficients has no effect in the microcalcifications detection.

In the experiments using the statistical test, all of the 18 malignant clusters are detected with the number of false positive results for some of them, table 1.

Normal mammographies		
Image number	Detection	
	skewness	kurtosis
1	0	0
2	0	0
3	0	0
4	0	0
5	0	0
6	0	0

Abnormal Mammograms				
Image number	Detection		Skewness and kurtosis detections	Identified Malignant regions [18]
	skewness	kurtosis		
7	1	1	same	1
8	4	4	same	4
9	1	1	same	1
10	2	2	same	1
11	2	2	same	2
12	1	1	same	1
13	2	2	same	2
14	2	2	same	1
15	4	4	same	1
16	4	4	same	2
17	4	4	same	2
18	2	2	same	2
19	1	1	same	1
20	6	6	same	6
21	3	3	same	1
22	2	2	same	1
23	2	2	same	1
24	4	4	same	1

Table 1: Performance using proposed detection methods on normal and abnormal mammographies

## References

- [1] Jöran Bergh, Fredrik Ekstedt, Martin Lindberg, *Wavelets*, Studentlitterature, Lund (1999).
- [2] Albert Boggess and Francis J. Narcowich, *A First Course in Wavelets with Fourier Analysis*, Prentice Hall (2001).
- [3] Ingrid Daubechies, *Ten Lectures on Wavelets* (1992).
- [4] David L. Donoho, *De-noising by Soft-Thresholding* IEEE Transactions on Information Theory, Vol. 41 No. 3, May 1995.
- [5] M. Garcia, A. Jemal, *Global Cancer Facts and Figures 2011*, Atlanta, GA: American Cancer Society (2011).
- [6] K.Kavitha, Dr.N.Kumaravel, *A Comparative Study of Various Microcalcification Cluster Detection Methods in Digitized Mammograms*, Department of Medical Electronics, College of Enguneering, Anna University, Chennai, India.
- [7] S. Malarvizhi, U. S. Ragupathy, A. Tamilarasi, *Mammogram Image Compression Using Multiwavelet Transform* , Department of ECE, Amrita Vishwa Vidyapeetham, Coimbatore (2009).
- [8] Mallat, S. *A Wavelet tour of signal Proccesing*, Academic Press, San Diego, 1998.
- [9] Martin Vetteli and Jelena Kovacevic, *Wavelets and Subband Coding*, Prentice Hall, New Jersey, 1995.
- [10] Y. Meyer, *Wavelets, Algorithms and applications*, SIAM, Philadelphia, 1993.
- [11] M. Nafi Gurcan, Yasmin Yardimci, A. Enis Cetin, and Rashid Ansari, *Detection of Microcalcifications in Mammograms Using Higher Order Statistics*, IEEE signal Processing Letters, VOL. 4, No. 8, August 1997.
- [12] M. Nafi Gurcan, Yasemin Yardimci, A.E. Cetin and R. Ansari, *Automated Detection And Enhancement of Microcalcifications in Mammograms Using Nonlinear Subband Decomposition*, Department of Electrical Engineering, Bilkent University, 1997.
- [13] C.L.Nikias, A.Petropulu, *Higher Order Statistical Analysis*, Prentice Hall, 19994.
- [14] K.Prabhu Shetty, V. R. Udupi and K. Saptalakar, *Wavelet Based Microcalcification Detection on Mammographic Images* , Intenational Journal of Computer Science and Network Security, VOL. 9 No. 7, July 2009.
- [15] Ted C. Wang , Nicolaos B. Karayiannis, *Detection of Microcalcifications in Digital Mammograms Using Wavelets*, IEEE Transactions on medical imaging, VOL. 17, No.4 (1998).
- [16] <http://en.wikipedia.org/wiki/Daubechies-wavelet>.

[17] <http://en.wikipedia.org/wiki/Skewness>.

[18] <http://marathon.csee.usf.edu/Mammography/Database.html>